Research Square

Preprints are preliminary reports that have not undergone peer review.
They should not be considered conclusive, used to inform clinical practice,
or referenced by the media as validated information.

LARP7 ameliorates cellular senescence and aging by allosterically enhancing SIRT1 deacetylase activity

Bing Zhang (bingzhang@sjtu.edu.cn)
Shanghai Jiao Tong University

Pengyi Yan
Xin Hua Hospital, Key Laboratory of Systems Biomedicine, Shanghai Center for Systems Biomedicine, Shanghai Jiao Tong University, Shanghai 200240

Zixuan Li
Xin Hua Hospital, Key Laboratory of Systems Biomedicine, Shanghai Center for Systems Biomedicine, Shanghai Jiao Tong University, Shanghai 200240, China

Junhao Xiong
Shanghai Jiao Tong University

Zilong Geng
Shandong University

Weiting Wei
Shanghai Jiao Tong University

Yan Zhang
Shanghai Jiaotong University School of Medicine

Gengze Wu
Daping Hospital, Third Military Medical University

Tao Zhuang
Shanghai East Hospital, Tongji University School of Medicine

Xiao Yu Tian
Chinese University of Hong Kong https://orcid.org/0000-0003-3472-9898

Zhijie Liu
The University of Texas Health Science Center at San Antonio https://orcid.org/0000-0001-6956-7839

Junling Liu
Shanghai Jiao Tong University School of Medicine

Kun Sun
Xinhua Hospital

Alex F Chen
Xinhua Hospital, School of Medicine, Shanghai Jiao Tong University

Yu Zhang

Key Laboratory of Arrhythmias of the Ministry of Education of China, Research Center for Translational Medicine, Shanghai East Hospital, Tongji University School of Medicine https://orcid.org/0000-0002-9570-1269

Chunyu Zeng

Daping Hospital, The Third Military Medical University https://orcid.org/0000-0003-0173-5028

Yu Huang

Chinese University of Hong Kong https://orcid.org/0000-0002-1277-6784

Article

Keywords: DNA Damage Response, Ataxia Telangiectasia Mutated Activation, Extracellular Shuttling, Vascular Aging, Atherogenesis

Posted Date: March 10th, 2021

DOI: https://doi.org/10.21203/rs.3.rs-275582/v1

License: This work is licensed under a Creative Commons Attribution 4.0 International License. Read Full License

LARP7 ameliorates cellular senescence and aging by allosterically enhancing SIRT1 deacetylase activity

Running title: LARP7 is a novel aging antagonist

Pengyi Yan[1†], Zixuan Ii[1†], Junhao Xiong[1†], Zilong Geng[1], Weiting Wei[1], Yan Zhang[2], Gengze Wu[3], Tao Zhuang[4], Xiaoyu Tian[5], Zhijie Liu[6], Junling Liu[7], Kun Sun[1], Fengyuan Chen[1], Yuzhen Zhang[4], Chunyu Zeng[3], Yu Huang[5], Bing Zhang[1*]

[1]Key Laboratory of Systems Biomedicine, Shanghai Center for Systems Biomedicine, Department of pediatric cardiology, Xin Hua Hospital, School of medicine, Xin Hua Hospital, Shanghai Jiao Tong University, 800 Dong chuan Road Shanghai 200240, China

[2]Renji-Med Clinical Stem Cell Research Center, Renji Hospital, School of Biomedical Engineering, Shanghai Jiao Tong University, Shanghai 200127, China

[3]Department of Cardiology, Chongqing Institute of Cardiology, Chongqing Cardiovascular Clinical Research Center, Daping Hospital, The Third Military Medical University, P.R. China

[4]Key Laboratory of Arrhythmias of the Ministry of Education of China, Research Center for Translational Medicine, Shanghai East Hospital, Tongji University School of Medicine, 150 Jimo Rd, Pudong New District, Shanghai, 200120, China

[5]School of Biomedical Sciences, Heart and Vascular Institute, Shenzhen Research Institute and Li Ka Shing Institute of Health Sciences, Chinese University of Hong Kong, Hong Kong, China.

[6] Department of Molecular Medicine, University of Texas Health Science Center, San Antonio, Texas 78229, USA.

[7]Department of Biochemistry and Molecular Cell Biology and Department of Pathophysiology, Key Laboratory of Cell Differentiation and Apoptosis of Chinese Ministry of Education, State Key Laboratory of Oncogenes and Related Genes, Shanghai Jiao Tong University School of Medicine, Shanghai, China.

†: Equal contribution

*: Correspondence

Abstract:

Cellular senescence is associated with pleiotropic essential physiopathological processes including aging and age-related diseases. The persistent DNA damage response (DDR) is a major stress leading to senescence, but the underlying molecular link remains elusive. Here, we identified La Ribonucleoprotein 7 (LARP7), a 7SK RNA binding protein, as a novel aging antagonist. DDR-mediated Ataxia Telangiectasia Mutated (ATM) activation triggered the extracellular shuttling and downregulation of LARP7, which dampened SIRT1 deacetylase activity, enhanced p53 and NF-κB transcriptional activity by augmenting their acetylation, and thereby accelerated cellular senescence. Deletion of LARP7 led to senescent cell accumulation and premature aging in rodent model. Furthermore, we show that this ATM-LARP7-SIRT1-p53/NF-κB senescence axis was active in vascular aging and atherogenesis, and preventing its activation substantially alleviated aging and atherogenesis. Together, this study identifies LARP7 as a gatekeeper for senescence, and the altered ATM-LARP7-SIRT1-p53/NF-κB pathway plays an important role in DDR-mediated cellular senescence and aging-related atherosclerosis.

Introduction:

Aging, defined as an age-dependent decline of cellular function, is related to many physiological processes including development, regeneration and wounding healing, and also to many pathologies such as cancer, neurodegeneration and atherosclerosis, etc [1]. Cellular senescence, a hallmark of aging, is generally sub-classified into replicative senescence (RS) and stress-induced premature senescence (SIPS) [2-4]. RS reflects a phenomenon that a primary nonmalignant cell stops proliferation and enters the senescent state after a limited number of replication (termed as Hayflick limit) [5], and is mainly attributable to the telomere attrition. SIPS is not induced by exhaustive cell passages or the telomere shortening, but rather by stressful insults including oxidative stress, oncogene activation, and persistent DNA damage response (DDR). RS and SIPS are not completely distinct and share some molecular pathways. For instance, DDR can be induced by telomere attrition or damage occurring during the cellular replication. Moreover, both RS and SIPS possess the same senescent traits: irreversible cell cycle arrest and proinflammatory secretory phenotype, termed the senescence associated secretory phenotype (SASP). Although there are variations, SASP factors usually comprise a panel of proinflammatory cytokines, chemokines, matrix metalloproteinases (MMPs) and growth factors that reinforce and spread senescence in an autocrine or paracrine manner [6,7]. Elimination of senescent cells and inhibition of SASP are proved to be effective to protect against aging and age-related diseases[8,9].

Persistent DNA damage and DDR activation induce cell cycle arrest and SASP, which are the leading cause for cellular senescence [10]. DDR activates the p53 (TP53) pathway by preventing MDM2-mediated p53 ubiquitination and degradation. This elevates the expression of $p21^{WAF1/Cip1}$ (CDKN1A), a direct target of p53, which suppresses CDK2 and halts the cell cycle at the G1 phase[11]. Moreover, DDR directly regulates senescence-associated inflammatory cytokine secretion. DDR activates ATM, which phosphorylates serine-85 of NF-κB essential modulator (NEMO), promotes its nuclear export, and subsequently activates the cytoplasmic IKK complex [11]. A recent study identified an alternative pathway centered on zinc finger transcription factor GATA4 that regulates SASP expression in some scenarios of senescence, which meanwhile suggests that our current understanding of the molecular mechanisms underlying DDR-mediated senescence are far from complete [12].

LARP7 is a La family RNA binding protein that binds 7SK RNA, one of the most abundant noncoding RNAs in cells. LARP7 forms a stable Ribonucleoprotein complex 7SK snRNP with Methylphosphate Capping Enzyme (MePCE) [13]. The well characterized function of 7SK snRNP is to imprison the positive RNAPII pausing release regulator-pTEFb and halt RNAPII transcription [14]. Genetic abrogation of LARP7 in mouse causes the embryonic lethality and primordial dwarfism. The recessive loss-of-function (LOF) mutations of LARP7 were also discovered in the familial probands with primordial dwarfism, intellectual disability, and Alazami syndrome [15-17]. However, the function of LARP7 in cellular senescence and aging remains unclarified.

Here, we report LARP7 as an effective protein allosteric activator of SIRT1. DNA-damaging inducers such as oxidative stress and irradiation reduce SIRT1 deacetylase activity through interruption of LARP7-SIRT1 interaction and subsequent activation of p53 and NF-κB pathway to accelerate cellular senescence and proinflammatory SASP. More importantly, our study demonstrates the activation of ATM-LARP7-SIRT1-p53/NF-κB -mediated senescent cascade promotes *in vivo* premature aging and aging-related atherogenesis. Taken together, our study uncovers a novel molecular pathway centered on LARP7 in DDR-mediated senescence and aging. The identification of this pathway advances our understanding of the cellular senescence and aging, and provides new opportunities for therapeutic intervention of aging and aging-associated atherosclerosis.

Results:

LARP7 is suppressed in premature and normal aging processes

The function of LARP7 remains largely unknown in cellular senescence and aging. Hence, we first examined the LARP7 expression in aged C57/BL6 mice. In multiple tested organs (aorta, skin, intestine, kidney, liver, brain, lung and spleen) of aged, 22-month-old mice,

LARP7 protein was significantly depressed compared to younger (6-month-old) mice (Figure 1A and Supplemental Figure 1A). However, the mRNA level was unaltered as revealed by reverse transcription-quantitative real-time PCR (RT-qPCR) (Supplemental Figure 1B). In aged aorta, LARP7 declined in both endothelium and smooth muscle (Figure 1B). To further gain insight into LARP7 expression in DDR-induced premature aging, we treated 2-month-old C57/BL6 mice with sublethal (7Gy) total body irradiation (TBI) [18,19]. Twelve weeks after IR treatment, the mice developed a significant aging phenotype, with grey coat color and increased $p16^{INK4A}$ (CDKN2A), a reliable marker of senescent/aged tissues, in both aorta (~1.8 fold) and skin (~2.1 fold) (Figure 1C and D, Supplemental Figure 1C-E). Similar to normal aging, LARP7 protein but not mRNA also significantly decreased in aorta and skin (Supplemental Figure 1C, E). Of note, LARP7 even started to decline 2 weeks after IR when aging had not yet become obvious, indicating that LARP7 downregulation was an early event.

The accumulation of senescent cells is the leading cause for aging [3]. Our *in vivo* expression data suggested that LARP7 may be also altered in senescent process. To test this likelihood, we examined the LARP7 expression in a replicative senescent model. Extensive replication of IMR90 cells led to their senescence starting at population doubling (PD) 39 and more notably at PD 56, as measured by the induction of $p21^{Waf1/Cip1}$ (CDKN1A) and $p16^{INK4A}$ [2,3](Figure 1E). Along with the emergence of senescence, LARP7 protein declined markedly at PD 39 and PD 56. (Figure 1E).

LARP7 deficiency accelerated senescence

Next, we set out to explore if LARP7 plays a role in cellular senescence. We stably knocked down LARP7 in low-passage primary IMR90 cells using two independently designed shRNAs. LARP7-depleted cells exhibited a flattened and enlarged morphology typical of senescence (Figure 2A and Supplemental Figure 2A). Senescence-associated β-galactosidase (SA-β-Gal) staining showing increased lysosomal content in LARP7-depleted IMR90 cells (Figure 2A and Supplemental Figure 2B). Senescence is usually associated with the global changes in epigenomic landscape, characterized by the formation of senescence-associated heterochromatin foci (SAHFs) [4]. We evaluated SAHF in IMR90 cells with repressive heterochromatin marker H3K9me3 and observed 2.1 and 2.5 folds increase respectively in the two shRNA cell lines (Figure 2A and Supplemental Figure 2B). Along with the heterochromatin structural change, loss of LaminB1, which promotes the rearrangement of H3K9me3 heterochromatin to form SAHFs [20], was also observed in LARP7-deficient IMR90 cells (Supplemental Figure 2A).

Using replication exhaustion assays, we found that LARP7 inhibition markedly accelerated the replicative senescence with reduced cell doubling times (Figure 2B), while ectopic expression of LARP7 apparently delayed it (Figure 2C). We further analyzed cell cycle

progression in LARP7-deprived cells using immunofluorescent staining for 5-ethynyl-2′-deoxyuridine (Edu, a marker for S phase) and phosphorylated histone H3 (pH3, a marker for G_2/M phase transition). These assays revealed dramatic reduction of DNA synthesis and mitotic activity in both LARP7-deprived IMR90 cells (Figure 2A and Supplemental Figure 2B). Together, these results indicated that LARP7 deprivation leads to halted cell cycle progression, consistent with replicative senescence.

To gain further insight into the underlying mechanism, we compared the transcriptome of LARP7-depleted IMR90 cells with wildtype cells using RNA sequencing (RNA-seq). A total of 288 differentially expressed genes (DEGs) were detected in LARP7-depleted IMR90 cells compared with wildtype cells (adj $p<0.05$, Supplemental Figure 2C). Gene Ontology (GO) analysis of these genes indicated significant enrichment in the terms of “Wound healing”, “Cell cycle arrest”, “Cytokine activity”, “Inflammatory response” and “Cellular senescence and aging” (Figure 2D). The enrichment of cell cycle regulators was further corroborated by gene set enrichment analysis (*P*=4.93E-10, NES=-2.6, Figure 2E). Among them, 21 core cell cycle regulators were significantly altered (Figure 2F). The expression of p21 (negatively regulates G_1/S phase transition) was upregulated, which was consistent with our staining results.

The alternation of inflammatory gene program indicates an onset of SASP that constitutes another hallmark of senescent cells. GSEA analysis of the LARP7 knockdown RNA-seq data set using a SASP gene set curated from the KEGG database showed that SASP genes were significantly enriched among upregulated genes (*P* value: 1E-10, NES: 3.13, Figure 2G). Among the 35 SASP genes that were upregulated in LARP7-knockdown IMR90 cells were canonical cytokines (IL1A, IL1B and IL6), chemokines (CXCL1, CXCL8 and CXCL10), growth factors (FGF2, BMP2) and matrix proteases (MMP1,2,3,10,12,14 &15), et. al (Figure 2H). We further confirmed the upregulation of these central SASP components (IL1B, IL6 and IL8) and cell cycle regulator p21 using RT-qPCR (Supplemental Figure 2D).

To rule out the possibility that activation of cell cycle regulators (CCR) and senescence programs upon LARP7 depletion was specific to IMR90 cells, we performed RNA-seq on wildtype and LARP7$^{-/-}$ MEF cells. A total 415 genes were differentially expressed in LARP7$^{-/-}$ MEF cells (Supplemental Figure 2E). GO analysis showed that DEGs were similarly enriched in gene sets “cell proliferation”, “inflammatory response” and “aging” (Supplemental Figure 2F). The enrichment of cell cycle and SASP genes were further validated by GSEA (Supplemental Figure 2G and H). Although the altered SASP and CCR genes did not exactly coincide between IMR90 and MEF cells, core CCR genes p21, CCNB1, CCNB2 and CDK1 were shared between cell types. Similarly, core SASP genes IL1B, CXCL1, IL6 and MMPs were altered in both cell types (Supplemental Figure 2I and J). Together, these data suggested that LARP7 deprivation led to cellular senescence by modulating the potent CCR and SASP pathways.

The declined SIRT1 deacetylase activity accounts for LARP7 depletion-induced senescence

The specific upregulation of p21 and SASP indicated activation of p53 (p53) and NF-κB pathways [21,22]. We measured the level of p53 and Rel-like domain-containing protein (RelA/p65), a key transcription factor in NF-κB pathway, in IMR90 cells after knocking down LARP7 for 3 days or 14 days. Surprisingly, at both time points, total p53 and RelA/p65 protein level were not significantly altered in three independent experiments (Figure 3A and B). Acetylation of p53 on Lys382 (p53-K382Ac) and p65 on Lys310 (p65-K310Ac) were reported to augment transcriptional activity of these proteins [22-24]. Therefore, we measured them using acetylation specific antibodies and found significantly increased acetylation of both residues (Figure 3C). Acetylation appeared rapidly by day 3 and was further elevated at day 14 after LARP7 shRNA knockdown. Consistent with p53 activation, p21, the direct transcriptional target of p53, substantially increased its expression at both day 3 and 14. In contrast, p16, not a direct downstream target of p53, only showed a late induction at day 14 (Figure 3A and B). In line with the acetylation of RelA/p65, the expression of IL1B, IL6 and IL8, central SASP factors activated by RelA/p65, were also upregulated. Together, these results suggest that activation of p53 and p65 via increased acetylation accounts for cell cycle arrest and SASP induced by LARP7 depletion.

Next, we sought to identify the enzymes responsible for regulating p53 and p65 acetylation levels downstream of LARP7. p300/CBP and histone deacetylase sirtuin1 (SIRT1) were suggested to modulate the acetylation of p53-K382Ac and p65-K310Ac [25-28]. We measured the expression of p300, CBP and SIRT1 by western blot. Protein levels of p300 and CBP did not change significantly in LARP7-depleted cells on both day 3 and day 14, whereas, SIRT1 was profoundly suppressed by day 14 (Figure 3A and B). Moreover, SIRT1 deacetylase activity markedly declined on day 3 by 1.6-fold, which was comparable to the effect of the SIRT1 inhibitor EX527, and became further reduced (2.4-fold) on day 14 (Figure 3D). These results suggested that SIRT1 deficiency may account for elevated p65 and p53 acetylation observed in LARP7-depleted cells. To further test this hypothesis, we treated LARP7 deficient cells with SIRT1-specific agonist SRT1720. Treatment for 12 hours was sufficient to abrogate the elevated acetylation of p53 and p65 (Figure 3E). Consistent with abrogated p53 and p65 acetylation, the induction of SASP factors (IL1B, IL6 and IL8) and p21 was also attenuated by SRT1720 (Figure 3F and G). Similarly, JSH-23, a NF-κB inhibitor also abolished the induction of SASP. More importantly, SRT1720 ameliorated the senescent phenotype of LARP7-depleted cells as indicated by SA-β-Gal staining (Figure 3H and I). Together, these results

suggested that the LARP7-SIRT1 axis mediates the acetylation and activation of p53 and p65, and which is pivotal for LARP7 depletion-induced senescence.

LARP7 allosterically enhanced SIRT1 deacetylase activity by interacting with its N-terminal allosteric activation domain.

LARP7 depletion reduced SIRT1 deacetylase activity, reflected by both SIRT1 activity measurement and elevated p53 and p65 acetylation, without significantly altering SIRT1 protein level at early stage. Moreover, the reservoir of nicotinamide adenine dinucleotide (NAD^+), a cofactor required for SIRT1 activity, was not affected by LARP7 depletion or overexpression in IMR90 cells (Supplemental Figure 3A). These results suggested that LARP7 may directly regulate SIRT1 activity. To further investigate this possibility, we used co-immunoprecipitation to determine if LARP7 and SIRT1 interact. We found that LARP7 co-precipitated SIRT1, and reciprocally SIRT1 co-precipitated LARP7 (Figure 4A). The interaction was not reduced by RNase A treatment (Figure 4A), and was recapitulated using bacterially purified, recombinant proteins (Supplemental Figure 3B), which suggest a direct interaction between LARP7 and SIRT1.

To determine which domain of SIRT1 interacts with LARP7, we used the domain deletion assay to measure the interaction of different SIRT1 regions with LARP7 (Figure 4B). SIRT1 residues 1-225 strongly bound LARP7, whereas residues 1-157 and 245-747 did not, indicating that residues 157-225 contain the interaction domain (Figure 4C). We confirmed this finding using bacterially purified recombinant proteins. SIRT1[158-225] (referred to hereafter as N-SIRT1) fused to GST pulled down full length LARP7 (Supplemental Figure 3C). Notably, N-SIRT1 is a conserved domain for allosterically enhancing SIRT1 deacetylase activity by interacting with some chemical agonists such as SRT1720 and protein agonist active regulator of SIRT1(AROS, also referred to as Ribosomal Protein S19 Binding Protein 1) [27,29]. These experiments provided us a clue that LARP7 may function like an activator to activate SIRT1 enzymatic activity allosterically [29]. To test this hypothesis, we evaluated SIRT1 deacetylase activity with or without LARP7 in test tubes using the *in vitro* SIRT1 activity assay. GST-LARP7 but not GST alone dose-dependently enhanced the deacetylase activity of purified full-length SIRT1 activity to a maximum of 2.4-fold basal levels. This stimulated SIRT1 activity was abrogated by deletion of the N-terminus of SIRT1 (Figure 4D and Supplemental Figure 3D). These results together demonstrate that LARP7 enhances SIRT1 activity by directly interacting with its N-terminal allosteric activation domain.

Next, we examined the effect of LARP7 on SIRT1 activity in a cellular context. We first purified Flag-tagged LARP7 and HA-tagged SIRT1 from 293T cells and then performed *in vitro* SIRT1 activity assay (Supplemental Figure 3E). As expected, the LARP7 yielded from mammalian cells enhanced SIRT1 deacetylase activity as well (Figure 4E). Similar to SIRT1

specific activator SRT1720, overexpressing wildtype LARP7 in IMR90 cells (LARP7^{OE} cells) significantly enhanced endogenous SIRT1 activity at both day 3 and day 14, which was comparable to 1μM SRT1720 treatment (Figure 4F).

To further testify if LARP7-modulated SIRT1 activation was able to promote the deacetylation of p53 and p65, we purified GST-p53 and GST-p65 from bacteria, and incubated the recombinant proteins with using p300 and acetyl-CoA to obtain GST-p53-K382Ac and GST-p65-K310Ac (Supplemental Figure 3F and G). Then, we performed *in vitro* deacetylation assays by incubating these substrates with SIRT1 and recombinant GST-LARP7. Wild-type SIRT1 catalyzed p53 and p65 deacetylation, which was stimulated by GST-LARP7 but not GST in a dose dependent manner (Figure 4G and H). We excluded contaminating deacetylases by performing parallel assays with catalytically inactive SIRT1-H363Y mutant protein, which did not alter p53 or p65 acetylation in the presence or absence of GST-LARP7 (Figure 4G and H).

Collectively, these data demonstrate that LARP7 allosterically activated SIRT1 deacetylase activity by binding to the N-terminal of SIRT1, which thereby induces the deacetylation of p53 and p65.

ATM regulates LARP7 stability and nuclear localization

We next sought to explore the mechanism of LARP7 downregulation in senescent cells and aging. DNA damage triggers persistent DDR and leads to cellular senescence and aging [3]. To test if DNA damage downregulated LARP7, we treated IMR90 cells with 10 Gy ionizing radiation (IR). This triggered rapid downregulation of LARP7 that was evident by one day after IR and reached a nadir by 3 days that was sustained through day 14 (Supplemental Figure 4A). Likewise, oxidative stress, a more common inducer of DNA damage in cellular senescence, profoundly depleted LARP7, as demonstrated by treatment of IMR90 cells with 100 μM H_2O_2 (Figure 5A). Unlike the rapid decrease of LARP7 induced by IR, H_2O_2-induced LARP7 depletion occurred more slowly but was equally severe by day 14. When we examined the subcellular localization of LARP7, we noted that both IR and H_2O_2 caused rapid LARP7 nuclear exclusion within 6 hours (Figure 5B and C, Supplemental Figure 4B and C).

ATM mediated-DDR is one of the main pathways for cellular senescence and aging [7,30]. To test if ATM activation is required for IR or H_2O_2-induced LARP7 degradation or nuclear exclusion, we pretreated IMR90 cells with 10 μM ATM inhibitor KU60019. KU60019 almost completely blocked LARP7 decline induced by both H_2O_2 and IR at both early (day 3) and late (day 14) time points (Figure 5D and Supplemental Figure 4D). KU60019 also halted the H_2O_2- and IR-induced exclusion of LARP7 from the nucleus (Figure 5B and C, Supplemental Figure 4B and C).

SIRT1 activity was attenuated in IR and ROS-induced senescence [31,32]. Given that LARP7 stimulates SIRT1 deacetylase activity, we hypothesized that LARP7 depletion triggered by IR and ROS may contribute to the attenuation of SIRT1 activity. To test this hypothesis, we first measured LARP7-SIRT1 interaction after H_2O_2 treatment. H_2O_2 markedly reduced LARP7-SIRT1 interaction, and this effect of H_2O_2 was blocked by KU60019 (Figure 5E). Consistent with the attenuated interaction, SIRT1 deacetylase activity was markedly suppressed by 100 μM H_2O_2 and IR in IMR90 cells, and this suppression was profoundly attenuated by the DOX-induced LARP7 overexpression (Figure 5F and Supplemental Figure 4E). KU60019 also recovered the SIRT1 activity in H_2O_2-treated IMR90 cells, which was further inhibited by knocking down LARP7, indicating that KU60019 recovered SIRT1 activity at least partially through LARP7 (Figure 5F and Supplemental Figure 4E). H_2O_2 induced acetylation of p53 and p65 on Lys382 and Lys310, respectively, which were also abrogated by LARP7 overexpression and KU60019 (Figure 5G and H). These changes in p53 and p65 acetylation were further mirrored in the expression of their downstream targets p21 (Figure 5I) and SASP factors (Figure 5J), and ultimately in the development of senescence, and measured by SA-β-Gal staining (Figure 5K and L). We performed similar studies of DNA damage elicited by IR, and found matching evidence of ATM-LARP7-SIRT1 axis linking DNA damage to cellular senescence (Supplemental Figure 4F and G). Together, these data demonstrate that the ATM-LARP7-SIRT1-p53/p65 axis is active and contributes to the DDR-induced cellular senescence.

LARP7 elimination leads to the premature aging phenotypes in mouse

Increased incidence of senescent cells contributes to aging and a wild range of age-related pathologies[2]. We next sought to explore if the LARP7-mediated senescence pathway contributes to aging phenotypes in vivo. Constitutive LARP7 knockout mice are not viable, so we crossed our previously reported conditional LARP7 flox allele with *UBC*^{CreERT2} mice [33], which broadly express tamoxifen-inducible Cre recombinase (CreERT2). We treated 2-month-old LARP7$^{flox/flox}$; *UBC*^{CreERT2} (abbreviated as LARP7^{iKO}) male mice with tamoxifen (TAM) every other day for 5 times to induce widespread inactivation of LARP7. We validated efficient Cre-mediated recombination of the LARP7^{flox} locus in all 8 tissues examined (Supplemental Figure 5A). Efficient recombination was reflected by extensive depletion of LARP7 mRNA and protein (Supplemental Figure 5B and C).

We monitored 43 wildtype (uninduced LARP7$^{flox/flox}$; *UBC*^{CreERT2}) and 43 LARP7^{iKO} mice to 14 months of age. 14-month-old LARP7^{iKO} mice showed signs of cachexia and loose hair (Figure 6A). In addition, LARP7^{iKO} mice gradually showed weight loss from 6 months after TAM treatment (Figure 6B). LARP7^{iKO} mice developed splenomegaly with significantly increased spleen mass compared to wild-type mice (2.1-fold, *P*=2.85E-10), suggesting

increased systemic inflammation (Figure 6C and D). Histological analysis of the skin showed reduced thickness of both the dermis and the subcutaneous adipose layers in LARP7^{iKO} compared to wild-type mice (Figure 6E and F). In a wound healing assay, LARP7^{iKO} mice had reduced ability to repair wounds (Figure 6G). Moreover, senescent cells accumulated in the four tissues assayed (kidney, brain, liver and lung), as determined by SA-β-Gal staining (from 2.3-fold to 5.1-fold increased staining intensity, P<0.0001 in all tested tissues) (Supplemental Figure 6A and B).

Blood vessels are prone to senescence and aging[34-36]. LARP7 was dramatically downregulated in the aortas of aged and IR-exposed prematurely aged mice compared to controls (Figure 1A, D). Thus, we carefully characterized the aging phenotype by isolating aortas from LARP7^{WT} and LARP7^{iKO} mice and found that the total weight of LARP7^{iKO} aortas were lower than LARP7^{WT} aortas (Supplemental Figure 6C). Histological analysis of thoracic aorta (TA) and left common carotid artery (LCCA) revealed a significant reduction in medial cell number and wall thickness and increased wall to lumen ratio in LARP7^{iKO} mice (Figure 6H and Supplemental Figure 6D-F). Elastica van Gieson (EVG) staining of elastic fibers revealed that in LARP7^{iKO} mice the elastic lamina was flattened and the intervals between elastic lamellae was much smaller (Figure 6H), suggesting that LARP7 depletion leads to loss of arterial elasticity and gain of vascular stiffness, the typical pathologies of vascular aging. In line with these degenerative vascular phenotypes, significantly increased accumulation of senescent cells was observed in both TA and LCCA of LARP7^{iKO} mice as evaluated by SA-β-Gal and p16 staining (Figure 6H, Supplemental Figure 6G and H).

In agreement with accumulation of senescent cells, typical SASP factors such as IL1b, IL6, Ccl2 (Mcp1), Mmp3, and Mmp9, and blood vessel-specific ones including intercellular adhesion molecule 1 (Icam1) and vascular cell adhesion molecule 1 (Vcam1) were significantly elevated, which suggest a proinflammatory environment in LARP7^{iKO} aorta (Figure 7A). Similarly, increased expression of p21 was also observed (Figure 7A). We next asked if elevated SASP and p21 expression were due to activation of p53 and p65 pathways, as we demonstrated in IMR90 cells. We compared the acetylation status of p53 and p65 in LARP7^{iKO} aorta with wildtype aorta and found that p53 and p65 acetylation were markedly increased in LARP7^{iKO} aorta (Figure 7B and C). Furthermore, short-term depletion of LARP7 for two weeks significantly elevated p53 and p65 acetylation (Figure 7B), suggesting that the elevated acetylation was directly regulated by LARP7 depletion. SIRT1 activity was also suppressed in both short-term and long-term LARP7-depleted aortas (Figure 7D). These results together suggest that the suppressive LARP7-SIRT1-p53/p65 pathway identified *in vitro* senescence contributes to the vascular aging and proinflammatory SASP *in vivo*.

Suppression of the LARP7-SIRT1 axis exacerbated atherosclerosis

Senescent ECs and VSMCs accumulate in atherogenic blood vessels [37] (Supplemental Figure 7A and B), which creates a proinflammatory environment, increases the uptake of plasma lipoproteins and promotes atherosclerosis [35,38]. LARP7 depletion accelerated vascular aging and inflammation, suggesting that it may exacerbate atherosclerosis. To test this hypothesis, we crossbred LARP7^{iKO} mice with ApoE^{KO} hyperlipidemic mice, a murine model frequently used to study atherogenesis[39]. LARP7^{WT}; ApoE^{KO} and LARP7^{iKO}; ApoE^{KO} mice were fed a high fat western diet (HFD) for 12 weeks to promote atherosclerosis (Figure 7E). Similar to LARP7^{iKO} mice, LARP7^{iKO}; ApoE^{KO} mice had substantially declined aortic SIRT1 activity (Figure 7F). To further probe the function of the LARP7-SIRT1 axis in atherogenesis, we administered the SIRT1 agonist SRT1720 to LARP7^{WT}; ApoE^{KO} and LARP7^{iKO}; ApoE^{KO} for 12 weeks along with HFD (Figure 7E). SRT1720 treatment increased SIRT1 activity in both wildtype and LARP7^{iKO}; ApoE^{KO} aortas (Figure 7F). No significant alterations of body weight and plasma cholesterol and triglyceride levels were observed between LARP7^{WT}; ApoE^{KO} and LARP7^{iKO}; ApoE^{KO} mice after 12 weeks of HFD (Supplemental Table 3). Although SRT1720 significantly reduced plasma cholesterol and triglyceride levels, there was no difference between LARP7^{WT}; ApoE^{KO} and LARP7^{iKO}; ApoE^{KO} mice. p16 immunostaining at the aortic root revealed emergence of senescent cells in the atherosclerotic lesion. Significantly, LARP7 deletion increased p16 positive senescent cells accumulation in aortic roots of LARP7^{iKO}; ApoE^{KO} mice (Figure 7G and H). In addition, Mac3 positive inflammatory cells were enriched in LARP7^{iKO}; ApoE^{KO} mice (Figure 7I and J), indicating increased F4/80^{+} macrophage infiltration. However, SRT1720 treatment reduced the senescent cells accumulation and inflammation at aortic root in LARP7^{iKO}; ApoE^{KO} mice comparing to those untreated mice (Figure 7G-J). Moreover, LARP7 deletion significantly increased atherosclerotic lesion area from 15.9 ± 2.4% to 26.7 ± 7.3% at 12 weeks, as measured by fractional area of the aortic luminal surface that was oil red-positive (Figure 7K and L). Similarly, LARP7^{iKO}; ApoE^{KO} mice exhibited increased lesion area at the aortic root (23.3 ± 2.3%, control vs. 37.7 ± 3.4%, LARP7^{iKO}; ApoE^{KO}; P=0.001, Supplemental Figure 7C and D). Consistent with the decreased senescent cells accumulation and inflammation, SRT1720 also reduced the atherosclerotic area in LARP7^{iKO}; ApoE^{KO} mice comparing to those untreated mice (Figure 7K and L, Supplemental Figure 7C and D).

These results together indicate that attenuation of the LARP7-SIRT1 axis exacerbates vascular senescence, inflammation and atherogenesis in the ApoE^{KO} lipidemic mouse model.

ATM inhibition alleviated the atherogenesis by recovering LARP7

ROS stimulates DNA damage and the subsequent DDR involving ATM activation, accelerates SIPS in vascular cells [40,41] and promotes atherogenesis. Dihydroethidium (DHE) staining of

freshly isolated aorta revealed marked elevation of ROS in the atherosclerotic aorta of $ApoE^{KO}$ mice fed with HFD, which activated ATM as revealed by the phosphorylated ATM staining (Figure 8A-D). In agreement with the *in vitro* results that ROS-mediated ATM activation suppressed LARP7, immunostaining showed that LARP7 was markedly repressed in atherosclerotic aortas of $ApoE^{KO}$ hyperlipidemic mice (Figure 8E and F). Moreover, a marked reduction of LARP7 was also observed in human atherosclerotic coronary artery but not in normal control coronary artery (Figure 8E and F) [42].

Therefore, we asked if the inhibition of ATM and DDR activation could reverse the downregulation of LARP7 in atherosclerotic vessels and thereby ameliorate atherogenesis. To this end, we treated $ApoE^{KO}$ mice with 5mg/kg KU60019 and fed them with HFD for 18 weeks (Figure 8G). To further understand the role of ATM-LARP7 axis in vascular senescence and atherogenesis, we also treated the $LARP7^{iKO}$; $ApoE^{KO}$ mice with KU60019 (Figure 8G). Western blot showed that KU60019 treatment successfully blocked ATM phosphorylation and increased LARP7 expression in the aortas of $ApoE^{KO}$ mice (Figure 8I). KU60019 increased SIRT1 deacetylase activity 1.5 folds in aorta and decreased the p53 and P65 acetylation (Figure 8H and I). Noteworthily, SIRT1 activity In KU60019-treated $LARP7^{iKO}$; $ApoE^{KO}$ mice was lower than in the KU60019-treated $LARP7^{WT}$; $ApoE^{KO}$ mice, indicating that ATM-mediated recovery of SIRT1 activity required LARP7 (Figure 8H). Similar results were also observed for p53 and p65 acetylation: KU60019 reduced p53 and p65 acetylation in KU60019-treated $LARP7^{iKO}$; $ApoE^{KO}$ aortas, but remained higher than in KU60019-treated $LARP7^{WT}$; $ApoE^{KO}$ aortas (Figure 8I). Changes in the expression of SASP genes and p21, p53 and p65 transcriptional targets, reflected these changes in the p53 and p65 acetylation (Supplemental Figure 8A).

Consistent with KU60019 reduction of cellular senescence in IMR90 cells, KU60019 alleviated cellular senescence in atherosclerotic lesions, and this affect was attenuated by LARP7 knockout (Figure 8J and K). In line with reduced expression of the SASP factors, KU60019 also significantly reduced the $F4/80^{+}$ microphage infiltration and inflammation within the lesion in $ApoE^{KO}$ mice as revealed by the macrophage specific marker (Mac3) staining, but that degree of reduction was not observed in $LARP7^{iKO}$; $ApoE^{KO}$ mice (Figure 8L and M). Moreover, KU60019 reduced the extent of atherosclerotic lesions in en face aorta (KU60019, 12.0 ± 2.0% vs vehicle, 25.0 ± 3.5%; P=0.001, Figure 8N and O) and in the aortic root (KU60019, 17.1 ± 2.9% vs vehicle 32.4 ± 1.9%; P=0.001, Supplemental Figure 8B and C), but the benefits of KU60019 was significantly compromised in $LARP7^{iKO}$; $ApoE^{KO}$ mouse ($ApoE^{KO}$ vs $LARP7^{iKO}$; $ApoE^{KO}$: 12.0 ± 2.0% vs 33.4 ± 5.9% in en face aorta; 17.1 ± 2.9% vs 34.7 ± 1.8% in the aortic root) (Figure 8N and O, Supplemental Figure 8B and C). Together, these results suggest that senescent pathway ATM-LARP7-SIRT1-p53/p65 axis first defined in the cellular

model also preserves in the atherogenic aorta, and contributes to the atherosclerotic senescence and lesion formation.

Discussion:

Senescence and premature aging are associated with many pathologies including cancer, diabetes and atherosclerosis et. al. However the molecular circuit underlying this important process remains largely unknown. Here, we unveil LARP7 functions as a pivotal hub in this circuit. Oxidative or genotoxic stress activates ATM that dampens LARP7-modulated SIRT1 deacetylase activity, increased p53 and p65 acetylation and transcriptional activity, and thereby promotes cell to undergo senescence. The activation of this pathway ATM-LARP7-SIRT1-p53/p65 not only promotes in vitro senescence, but also deteriorates in vivo aging and aging-related atherosclerosis. On the contrary, preventing the activation of this pathway ameliorates the vascular aging and atherosclerotic lesion growth profoundly. Altogether, we identify a new pathway ATM-LARP7-SIRT1-p53/p65 centered on LARP7 that governs the DDR-mediated senescent progression (Supplemental Figure 9).

Sirtuin family genes are the major players regulating organism aging[1]. Yeast silent information regulator 2 (SIR2) is able to increase the lifespan of yeast and worm [43 44]. In mammals, enhancing the activity of SIRT1, the closest ortholog of SIR2, improves multiple aspects of health related to aging though it is debatable as to whether it can increase the longevity [45 46]. SIRT1 is a NAD^+-dependent class III histone deacetylase, whose deacetylase activity is tightly regulated within the cells either by the level of enzymatic cofactors such as NAD^+ or by the protein modulators. Deleted in breast cancer 1 (DBC1) is a negative protein regulator for SIRT1. DBC1 directly binds to SIRT1 HDAC domain via a short leucine zipper motif which blocks the access of substrates such as p53 and FOXO3A to the deacetylase catalytic domain and therefore halt their deacetylation. A recent study found human immunodeficiency virus type1 (HIV1) Tat protein also can bind to HDAC domain and halts SIRT1 to deacetylate the NF-κB p65 subunit during the HIV infection. Before our study, AROS is the only positive cellular regulator of SIRT1 identified by a yeast two-hybrid screening. AROS binds to the N-terminal domain and induces the confirmation change of SIRT1 that allosterically increases the HDAC domain deacetylase activity. Here, we identify LARP7 as the secondary cellular protein activator of SIRT1. LARP7 binds to the same N-terminal domain of SIRT1 and enhances the deacetylase activity, which indicates these two protein activators share the same activation mechanism. However, AROS-mediated deacetylation of p53 is weak and cell-context dependent, and no study show AROS can mediate the deacetylation of p65. Moreover, AROS has not been identified to involve in regulation of cellular senescence. These lines of evident LARP7 is possibly a more general and robust SIRT1 activator comparing with AROS.

Many studies report that SIRT1 deacetylase activity substantially declines during senescence and aging, and which accelerates their progression. Likewise, the present results show SIRT1 activity is decreased in the H_2O_2-, IR- and LARP7 depletion-induced senescence. We further unveil that SIRT1 activity declines very rapidly: 3 days after LARP7 knockdown or 1 days after H_2O_2 and IR treatment, which is in contrast to much later downregulation of SIRT1 protein 14 days after LARP7 knockdown. Intriguingly, LARP7 also diminishes very rapidly- 1 day after the IR or 3 days after H_2O_2 exposure. An even more rapid extranuclear shuttling of LARP7 occurs 6 hours after H_2O_2 and IR treatment, which significantly dampens the LARP7-SIRT1 interaction. The declined cofactor NAD^+ level is thought be the major reason for declined SIRT1 activity in aging, however, we didn't observe a significant NAD^+ haploinsufficiency after knocking down LARP7 for up to 3 days. Regarding all these lines of evident, we believe that the rapid loss of SIRT1 deacetylase activity at the beginning of DDR and DDR-induced senescence is most likely attributed to the swift downregulation and translocation of LARP7. The attenuated SIRT1 activity is pivotal for senescence and aging development [1]. The early suppression of SIRT1 activity mediated by LARP7 may serves as a trigger to elicit senescence, therefore, possessing the unique importance in the onset of senescence. This is further supported by our multiple *in vitro* and *in vivo* experiments that clearly showing manipulating LARP7 level can either cause or prevent the senescence and aging further support this deduction. It is worthy to mention here that our results show LARP7 is depleted throughout the aging process, indicating it also contributes to the sustained suppression of SIRT1 activity during aging.

Accumulative DNA damage and DDR have been related to atherogenesis. Using the DNA markers of 7,8-dihydro-8-oxo-2'-deoxyguanosine (8-oxo-dG) and rH2A.X, and phosphorylated ATM, multiple studies report the DNA damage and persistent DDR exists in the senescent cells within the atherosclerotic lesion, particularly in the advanced plague[35]. The accumulated senescent cells facilitate the atherogenesis as revealed by multiple previous study. However, the detail molecular mechanism remains unclarified. We found elevated ROS and pATM in atherosclerotic lesion originated from lipidemic $ApoE^{KO}$ mice, and accordingly, where LARP7 and SIRT1 activity are substantially suppressed. Noteworthily, in agreement with our *in vitro* results, genetic ablation of LARP7 results in the declined SIRT1 activity, elevated p53/p65 acetylation and increased expression of SASP and p21 that leads to the aggravated vascular aging in normal mice, and atherogenesis in the lipidemic $ApoE^{KO}$ mice. In contrast, blocking the transduction of this pathway using ATM inhibitor, LARP7 overexpression or SIRT1 activator significantly halts p53/p65 acetylation and SASP and p21 expression, and ultimately ameliorates the vascular senescence and atherogenesis. These results suggest that this newly defined senescent pathway ATM-LARP7-SIRT1-p53/65 plays an irreplaceable role in DDR-induced vascular aging and atherogenesis. Vascular atherosclerosis are the most

widespread diseases across the world. Our study shows that three independent approaches of ATM inhibitor, genetic restoration of LARP7 and SIRT1 chemical agonist can all efficiently protect against atherosclerosis, indicating targeting ATM-LARP7-SIRT axis hold a potency for therapeutic management of this highly prevalent disease.

In summary, the present study reveals a previously un-recognized aging pathway ATM-LARP7-SIRT1-p53/65, which may serve as new therapeutic targets against aging and aging-related diseases.

Methods

Experimental animals

LARP7$^{flox/flox}$ mouse was reported in our previous study. UBC^{CreERT2} mice (129S.Cg-*Ndor1* $^{Tg(UBC-cre/ERT2)1Ejb}$/J, 007179) were purchased from the Jackson Laboratory. The inducible LARP7 loss-of-function mice were generated by crossing LARP7$^{flox/flox}$ with UBC-Cre/ERT2 mice. ApoE^{KO} mice (C57BL/6-Apoe^{em5Smoc}, NM-KO-190565) were purchased from Shanghai Biomodel Organism Science & Technology Development corporation (Shanghai, China). All animal protocol and procedures were approved by Institute Animal Care and Use Committee (IACUC) of Shanghai Jiao Tong University. The mice were housed under standard conditions with a 12-hour light/dark cycle, and had free access to water and standard chow unless specified.

Human coronary artery samples:

Human coronary artery samples were acquired from the University of Pennsylvania Human Heart Tissue Bank and kindly provided by Yuzhen Zhang (Shanghai East Hospital, Tongji University School of Medicine).

Aging studies

For normal aging study, C57BL/6J mice were obtained from Lingchang BioTech mice, maintained in a standard feeding and house condition and sacrificed until 6 or 22 months of age. For LARP7^{iKO} mice, 2 months old LARP7$^{flox/flox}$; UBC-Cre/ERT2^{+} male mice were randomly assigned to two experimental groups and injected with sunflower seed oil or tamoxifen (50 mg/kg mice, every other day for total 5 times) intraperitoneally. Following the final tamoxifen injection, mice were monitored weekly and the body weight were recorded monthly. For IR-induced aging study, 2-month-old C57BL/6J male mice were exposed to X-ray (7Gy) for one time. The tissues were collected 2 weeks or 12 weeks following irradiation.

Atherosclerosis studies:

The LARP7$^{flox/flox}$; UBC-Cre/ERT2 mice were crossed with ApoE^{KO} hyperlipidemic mice to generate LARP7 knockout hyperlipidemic mice (LARP7^{iKO}; ApoE^{KO}). The mice of 6 to 8 weeks were randomly assigned to experimental groups and injected with tamoxifen (50 mg/kg mice, every other day for total 5 times) intraperitoneally. LARP7^{iKO}; ApoE^{KO} mice were fed with a

western diet (Research Diets, D12108C) with 40% fat and 1.25% cholesterol for 12 weeks or 18 weeks respectively before being sacrificed. For drug rescue experiments, SRT1720 was resolved in solution (2% DMSO + 30% PEG300 + 1% Tween80), KU60019 was resolved in solution (5% DMSO + 30% PEG300), and SRT1720 (2 mg/kg) and KU60019 (5 mg/kg) were injected intraperitoneally every other day for 12 weeks or 18 weeks.

An Oil Red O whole-mount staining of isolated aorta was deployed to reveal the atherosclerotic lesion on the aorta *en face, and* Oil Red positive region relative to the entire aortic area was calculated with Image J. For the Oil Red O staining of aortic roots, we used the first cryosection capturing all 3 leaflets of the aortic valve collected from the side of aortic arch, and the adjacent two sections were used for Mac3 and p16 immunostaining respectively. This section point was defined as zero point, two serial sections either proximal and distal to the zero point with 80um intervals were also stained. The average fluorescent intensity of 5 serial sections was subjected for the calculation. All the quantifications of aorta *en face* and aortic root were performed by experimenter who were blinded to the group design.

Plasmatic cholesterol and triglyceride

Blood samples were collected into heparin-coated tubes and centrifuged at 1500 rpm for 10 min to harvest the plasmas. Total plasma cholesterol and triglyceride were measured using Total Cholesterol Quantification Kit (A111-1-1, Nanjing Jiancheng Bioengineering Institute) and Triglyceride Quantification Kit (A110-1, Nanjing Jiancheng Bioengineering Institute) respectively according to the manufacturer's instructions.

Cell culture

IMR90 human diploid fibroblast line was purchased from ATCC (CCL-186) and grown in MEM medium (Gibco) supplemented with 10% fetal bovine serum (FBS), L-glutamine, sodium pyruvate, nonessential amino and sodium bicarbonate. The purification of MEFs was performed as previously described[47]. HEK293T cells were provided by William T. Pu lab (Harvard University). MEFs and HEK293T cells were cultured in DMEM medium (Gibco) supplemented with 10% FBS. All of the cells were incubated at 37˚C under 5% CO_2.

Generation of stable cell lines

The IMR90 stable cell lines were generated with lentivirus infection. Lentivirus production followed the protocol we described previously [48]. In brief, lentiviral shuttle plasmid containing LARP7 shRNA or cDNA together with helper vectors of psPAX2 and pMD2.G were co-transfected to HEK293T cells using 1 mg/ml PEI (polyethylenimine, Biopolymer). 48h and 72h after transfection, the culture medium containing viral particles was collected, centrifuged and passed through 0.45 μm filters to remove cell debris. The virus was precipitated with 8.5% PEG6000 and suspended in PBS. The virus titer was estimated with a Lenti-X™ p24 Rapid Titer kit (Takara Bio).

To generate the LARP7-depleted stable cell line, IMR90 fibroblasts (~15 population doublings) were infected with 1-3 MOI of pLKO.1-LARP7 shRNA or pLKO.1-scrambled shRNA lentivirus for 24h, and then selected with 1 μg/ml puromycin for 7 days. The survived cells were maintained and passaged in the culture medium supplemented with 0.2 μg/ml puromycin. To generate doxycycline-inducible LARP7 expression cell line, IMR90 fibroblasts (population doublings ~ 15) were co-transduced with pLenti-CMV-TRE3G-Neo-GFP-LARP7 and pLenti-CMV-rtTA3G Blast lentiviruses for 24 hours, and then selected with both 200 μg/ml G418 (Thermo Fisher) and 1.5 μg/ml blasticidin (ant-bl-05, InvivoGen) for 7 days. The survival clones were propagated in the culture medium supplemented with 40 μg/ml G418 and 0.2 μg/ml blasticidin for another 14 days. LARP7 expression was induced by 1 μg/ml doxycycline (Sigma-Aldrich).

Population doubling assay

IMR90 fibroblasts were cultured under normal conditions. Stable IMR90 cells were seeded at a density of $2x10^5$ cells per 6 cm dish for the first five passages, and $4x10^5$ cells per dish for the remaining passages. The PD was calculated as $\log_2(D/D_0)$, here, "D" reflected the density of cells when harvesting, and "D_0" reflected the density of cells when seeding.

Plasmids:

HA-tagged SIRT1 (1-747, 1-157, 1-225, 1-244, 511-747, 245-747, 158-225), Flag-tagged full-length LARP7 were subcloned into pHAGE-CMV-MCS-IRES-ZsGreen vector. LARP7 (1-580), SIRT1 (1-747, 245-747 and 158-225), p53 and p65 were subcloned into pGEX6P1 vector. pGEX6P1 SIRT1 H363Y mutant was constructed using *Fast* Mutagenesis System kit (TransGen Biotech, FM111). To obtain the doxycycline-inducible LARP7 construct, Flag-tagged LARP7 was cloned into pLenti-CMV-TRE3G-Neo-GFP-Lamin A (addgene, #118709) to replace LaminA. pLenti-CMV-rtTA3G-Blast was purchased from addgene (#26429). The synthesized short hairpin RNAs (shRNAs) against LARP7 were cloned into pLKO.1 vector. shRNA sequences used for cloning were included in Supplementary Table 2.

Protein analysis

Western blotting:

Cells or tissues were lysed in high-salt buffer B (20 mM HEPES pH7.9, 450 mM NaCl, 25% Glycerol, 0.2 mM EDTA, 0.5 mM DTT, 1% NP40, 0.5% SDS) with protease inhibitors for 20 min on ice. The isolated proteins were separated on SDS-PAGE gels and transferred to 0.45 μm PVDF membrane. The membrane was blocked with 5% BSA in TBS/0.1% Tween 20 (TBST), and then sequentially incubated with primary antibodies (Supplementary Table 4) and horseradish peroxidase-conjugated secondary antibodies (Cell Signaling Technology). The blots were imaged within Amersham Imager 600 after developing with enhanced chemiluminescence substrate (Immobilon Western, WBKLS0500, Millipore).

Immunoprecipitation:

Immunoprecipitation was performed as previously described[47]. Briefly, cells were lysed with buffer A (10 mM HEPES pH7.9, 10 mM KCl, 1.5 mM MgCl2, 0.05% NP40 and 0.5 mM DTT) on ice for 10 min, centrifuged at 3000 rpm for 5 min, and the precipitated nuclear pellets were further lysed in high salt buffer B for 20 min. The nuclear extract was incubated with primary antibodies overnight at 4˚C and then pulled down with protein G Dynabeads (Thermo Fisher, 10004D), or directly pulled down by Flag antibody-conjugated M2 agarose beads (Sigma-Aldrich, M8823) or HA magnetic beads (Thermo Fisher, 88837) at 4˚C for 4 h. After washing with cold PBS for three times, beads-bound protein complexes were boiled with 4x Laemmli buffer and detected with corresponding antibodies.

Expression and purification of the recombinant protein:

The corresponding expression plasmids were transformed into BL21/DE3 E. coli cells and induced with isopropyl-β-D-thiogalactopyranoside (IPTG) (0.5 mM for GST-tagged full-length or domain deletions of LARP7 and His-tagged LARP7, GST-tagged p53, p65; 0.2 mM for GST-tagged full-length, domain deletion or mutation of SIRT1) for overnight at 18˚C. The following operations were performed in a 4˚C chamber. For GST-tagged full-length, domain deletion or mutation of SIRT1, bacterial cell pellets were resuspended with buffer (50mM Tris-HCl PH8.0, 250mM NaCl, 5mM β-mercaptoethanol) with cOmplete^{TM} protease inhibitors cocktail (Sigma-Aldrich) and Benzonase nuclease (Sigma-Aldrich). For GST-tagged LARP7, His-tagged LARP7, GST-tagged p53 and p65, bacterial cell pellets were resuspended with 1X PBS containing protease inhibitors and benzonase nuclease. Suspended cells were lysed with a Constant Cell Disruption System and centrifuged at 10,000 rpm for 30 min to remove the cell debris. For GST-tagged protein purification, the supernatant was loaded onto Glutathione-Sepharose agarose (GE Healthcare, 17-0756-01) and washed with the corresponding suspended buffer extensively. The recombinant proteins were eluted with buffer (50mM Tris-HCl PH8.0, 10mM reduced Glutathione, 150mM NaCl) and proceeded to dialyze in PBS overnight. GST-tagged full-length or domain deletion or mutation of SIRT1 proteins were digested by 3C protease during dialysis before the subsequent activity assay. For purification of His-tagged LARP7, the supernatant was incubated with TALON Metal Affinity Resin (Clontech, 635501), washed with buffer (20 mM Tris-HCl pH7.4, 150 mM NaCl and 10 mM imidazole) for 5 times, eluted with the buffer (20 mM Tris-HCl pH7.4, 150 mM NaCl and 200 mM imidazole) and subjected to dialysis in cold PBS overnight. Following the dialysis, the recombinant proteins were concentrated with Amicon column (Millipore), resuspended in PBS containing 10% glycerol, aliquoted and stored at -80 ˚C.

GST-pulldown assay

5 μg of purified His-tagged LARP7 protein was incubated with GST, 158-225 or 1-747 of GST-SIRT1 bound with glutathione-Sepharose 4B beads within the binding buffer (1X PBS pH 7.4, 1% Triton X-100) containing protease inhibitors at 4˚C for 2 h. Following the incubation, the beads were rinsed with 1x PBS for 3 times, boiled in 4x Laemmli buffer and analyzed by Western blotting.

SIRT1 activity assay:

SIRT1 activity was determined by a Universal SIRT Activity Assay Kit (ab156915, Abcam) according to the manufacturer's protocol. For in vivo SIRT1 activity assay, cells or tissues were first homogenized in buffer A (10 mM HEPES pH7.9, 10 mM KCl, 1.5 mM MgCl2, 0.05% NP40 and 0.5 mM DTT) to remove the cytoplasmic protein and then lysed with buffer B (20 mM HEPES pH7.9, 450 mM NaCl, 0.5 mM DTT). An equal amount of extract was directly subjected to the assay after measured with BCA assays. For in vitro SIRT1 activity assay, purified SIRT1 protein together with indicated recombinant proteins were incubated with substrate and assay buffer for 90 mins at 37˚C.The absorbance at 450nm was read in BioTeK microplate reader. The SIRT1 activity was calculated using the following formula: SIRT1 activity (OD/min/mg) = $\left(\frac{\text{Sample OD - NNC OD}}{\text{Protein amount (μg)} \times \text{Incubation time (min)}}\right) \times 1000$. Here, NNC denotes control wells with no SIRT co-factor NAD^+.

In vitro acetylation and deacetylation assay:

HEK293T cells were transfected with HA-tagged p300 plasmids and lysed with high salt buffer B (20 mM HEPES pH7.9, 450 mM NaCl, 25% Glycerol, 0.2 mM EDTA, 0.5 mM DTT, 1% NP40, 0.5% SDS). Cell extracts were immunoprecipitated with HA agarose beads, washed with cold PBS for three times and resuspended in 5× HAT buffer (50 mM Tris-HCl pH 8.0, 10% glycerol, 0.1 mM EDTA and 1 mM DTT). For in vitro acetylation assay, recombinant GST-tagged p53 or p65 protein was incubated with HA-p300 beads, 100 μM acetyl-CoA (Sigma, A2181) in 1 X HAT buffer at 37˚C for 45 min. The acetylated p53 and p65 were evaluated by western blotting after removal of beads-bound p300. For in vitro deacetylation assay, acetylated GST-tagged p53 or p65 was incubated with purified SIRT1 or SIRT1 H363Y protein and with indicated recombinant proteins in deacetylation buffer (50 mM Tris-HCl pH 8.0, 137 mM NaCl, 2.7 mM KCl, 1mM $MgCl_2$, 1 mg/ml BSA, 10% glycerol) containing 3 mM NAD^+ and 200 nM TSA (inhibition of class I/II HDAC) at 37 ℃ for 1 h. Following deacetylation assay, protein samples were boiled with 4x Laemmli buffer and immunoblotted with corresponding antibodies.

NAD^+ measurement

The NAD/NADH ratio was determined by NAD/NADH Quantification Kit (Sigma, MAK037) according to the manufacturer's protocol. Briefly, $2x10^5$ IMR90 cells were lysed in NADH/NAD extraction buffer by replicative freeze/thawing for 2 cycles, and then centrifuged at 12000 rpm for 10 min to remove the insoluble materials. To detect total NAD, purified cell lysates were

mixed with NAD Cycling Buffer containing Cycling Enzyme Mix and incubated at room temperature for 5 mins and then with NADH Developer for 1-4 hours at room temperature. After terminated with Stop solution, the absorbance at 450nm was measured in BioTek microplate reader. To measure the NADH only, NAD in cell lysates was decomposed by heating to 60 °C for 30 min before detection. The method detecting NADH is same to NAD. A standard curve was established by measuring a serial dilution of NADH standards. The ratio of NAD/NADH was determined by the following equation: ratio = $\frac{NAD_{total}-NADH}{NADH}$. Here, NAD_{total} denotes the amount of total NAD (NAD + NADH); NADH denotes the amount of NADH, both were calculated from the standard curve.

Wound healing analysis:

The meddle dorsal skin of anesthetized mice was introduced to a 3-mm biopsy wounds with biopsy skin perforator. The wound diameter was gauged by a digital caliper for a following period of 7 days.

Histology:

Dorsal skin was dissected, fixed in 4% paraformaldehyde and embedded in paraffin. 5 μm sections were stained with hematoxylin and eosin following the standard procedure. The thickness of the dermal and adipose layers was calculated using ImageJ software (NIH). For quantification of each mouse, we used 20 serial sections. The average thickness of the dermal and adipose layers area was presented.

The thoracic aorta (TA) and left common carotid artery (LCCA) of mice were isolated and freshly embedded in O.C.T. compounds (Tissue-Tek). 8 μm cryosections were fixed with 4% paraformaldehyde and then stained with hematoxylin and eosin (HE), Elastica van Gieson (EVG) Stain Kit (Shanghai Rongbio) or Picrosirius Red Stain Kit (Yeasen Biotech) by following the manufacturer's instruction. The average signals from 10 sections with 8 μm intervals in each mouse were calculated.

Oil Red O staining:

For the whole mount staining, mice aortas were dissected in cold PBS and fixed in 4% paraformaldehyde at 4˚C for 24 h. For the staining of aortic root, cryosections were fixed in 4% paraformaldehyde at room temperature for 15 min. Samples were first rinsed in water for 5 min and then in 60% isopropanol for 5 min. The aortas and aortic roots were stained with 0.2% Oil Red O (Sigma, O0625) for 1 h with gentle shaking at room temperature, rinsed again with 60% isopropanol for one time, and then with water for three times. The stained aorta en face was cut opened, fixed on a black plate with the endothelium facing upwards and captured with a Nikon DS-Ri2 stereotype microscope. The image of aortic root section was captured with a Nikon & NI-U upright microscope. The lesion area was quantified by using ImageJ package.

SA-β-Gal staining:

The β-galactosidase activity was evaluated with Senescence β-Galactosidase Staining Kit (Cell Signaling Technology, #9860) according to the manufacturer's instruction. Cells were fixed with 4% paraformaldehyde for 20 min, washed twice with PBS and incubated with X-Gal solution (pH 6.0) at 37˚C for overnight. Tissues were freshly frozen in O.C.T. compounds, cryosectioned and fixed with 4% paraformaldehyde for 15 min at room temperature. After washing twice with PBS, the sections were stained in X-Gal solution (pH 6.0) at 37˚C for variable time: 12 hours for aorta and kidney, 36 hours for lung, 48 hours for liver and brain. SA-β-Gal positive cells or tissues were captured using a Nikon & NI-U Microscope and quantified by ImageJ.

Immunofluorescence:

Cells cultured on glass coverslips were fixed with 4% paraformaldehyde at room temperature for 10 min. Tissue cryostat sections from -80˚C were dried in air at room temperature for 10 min, fixed in pre-cold 1:1 methanol/acetone for 10 min at -20˚C, dried in air for 10 min and followed by rehydration in PBS for 5 min. For paraffin section, paraffin-embedded human coronary artery samples were dewaxed in xylene and rehydrated in gradient alcohols. The antigen retrieval was performed in citrate retrieval buffer (10mM sodium citrate pH 6.0) at 95˚C for 20 min. After being blocked with blocking buffer (5% normal donkey serum, 1% BSA and 0.3% Triton X-100 in PBS) for 30 min at room temperature, the cells or tissue sections were incubated with 1:200~1:100 primary antibodies (See supplementary table 4) in dilution buffer (5% normal donkey serum, 1% BSA and 0.1% Triton X-100 in PBS) for overnight at 4 ℃, and then with Alexa Fluor 488-, 555- and 647-conjugated secondary antibodies (1:200, Thermo Fisher Scientific) for 1 h at room temperature. Hoechst 33342 (Thermo Fisher Scientific) was used for nuclear staining.

Immunohistochemistry:

Cryosections of mouse aortas were fixed in cold 1:1 methanol/acetone for 10 min at -20˚C, dried in air for 10 min and then quenched with 3% H_2O_2 in methanol for 20 min. After blocking with 2% horse serum, the sections were sequentially incubated with 1:200 pATM antibody (Supplementary Table 4), universal biotinylated secondary antibody (Vector Laboratories, PK-7200) and R.T.U. VECTASTAIN ABC Reagent (Vector Laboratories, PK-7200). The sections were color-developed with ImmPACT DAB Substrate (Vector Laboratories, SK-4105) and counterstained with hematoxylin to reveal the nuclei. A Nikon & NI-U Microscope Camera was used to record the stained sections.

RT-qPCR

Total RNA was extracted from tested cells or tissues by using RNAsimple Total RNA Kit (TIANGEN Biotech) according to the manufacturer's instruction. 1-5 μg of RNA were reversed transcribed to cDNA using a Hifair II First Strand cDNA Synthesis Kit (gDNA digester plus) (YEASEN) and quantified by the real-time PCR using Hieff® qPCR SYBR Green Master Mix

(High Rox Plus) (YEASEN) in ABI Prism 7500 instruments. Sequence-specific primers used for quantitative real-time PCR were documented in Supplementary Table 2.

RNA-Seq

Total RNA was purified from IMR90 and MEFs using RNeasy Miniprep Kit (Qiagen) with an on-column DNase I digestion to eliminate residual DNA. RNA-Seq was performed at Novogene Corporation (Shanghai). Briefly, mRNA was purified from 1.5 mg of total RNA using poly-T oligo magnetic beads, and the libraries were constructed with NEBNext Ultra^{TM} RNA library Prep Kit customized for Illumina (NEB). The library quality was assessed with Agilent Bioanalyzer 2100 system. Illumina HiSeq 4000 platform was deployed to generate 150 nt paired-end reads

RNA-sequencing analysis

The quality control of FASTQ files was performed with FastQC. The alignment of FASTQ files to hg19 genome was performed with HISAT2 (http://daehwankimlab.github.io/hisat2/). HTSeq (https://github.com/htseq/htseq) was used to count the numbers of reads mapped to each gene. The gene expression was normalized as counts per million (CPM). The DEGs (differentially expressed genes) were identified by R package DESeq2 with an adjusted p-value less than 0.05 and log2 fold change greater than 0.585. GSEA analysis was performed using the gene set of SASP or cell cycle regulator (Detail gene list in Supplementary Table 1). GO analysis was carried out with DAVID algorithm (https://david.ncifcrf.gov/).

Statistics

Each assay was repeated at least three times independently. The data were presented as Mean ± Standard Deviation (SD). Comparisons between two groups were analyzed by two-tailed parametric t test if the data were normally distributed, otherwise, the Mann-Whitney U test was employed. Differences between multiple groups were performed using one-way ANOVA followed by Tukey post-hoc tests. Statistical analysis was performed using GraphPad Prism 8 or Microsoft Excel. The detail biological replicates in each group were indicated in figure legends. A difference was considered significant if $P<0.05$.

Supplemental information

Supplemental data include four tables and nine figures.

Data accessibility:

All the RNA sequencing raw and processed data were deposited to GEO database (GSE 160279) with a secure token “qtovsgyynhezlct”

Acknowledgements

We sincerely thank Dr. William T. Pu (William T. Pu lab, Harvard Medical School) for helping revising the paper, thank Wei Deng & Ming Lei (Medical School of Shanghai Jiao Tong University) for helping with protein purification and enzymatic activity measurements.

B.Z. is supported by the National Key Research and Development Program of China (2018YFC1312702 and 2018YFC1002400), National Science Foundation of China (91539109, 31671503, 91939302 and 31872836), a Thousand Young Talents Award (16Z127060017), and the Innovation Program of the Shanghai Municipal Education Commission (2017-01-07-00-01-E0028).

Contributions

B.Z. conceived and supervised this study. P.Y.Y., Z.X.L., J.H.X., W.W.T. performed the wet experiments. Z.L.G. performed the computational analysis of the RNA-seq data. Y.Z. assisted with the aging phenotype characterization. G.Z.W., T.Z., X.Y.T., Y.Z.Z. assisted with the atherosclerosis assays. J.L.L., K.S., F.Y.C., Y.Z.Z., C.Y.Z., Y.H. reviewed and revised the paper. P.Y.Y. and B.Z. wrote the paper.

Competing interests

None

Figures:

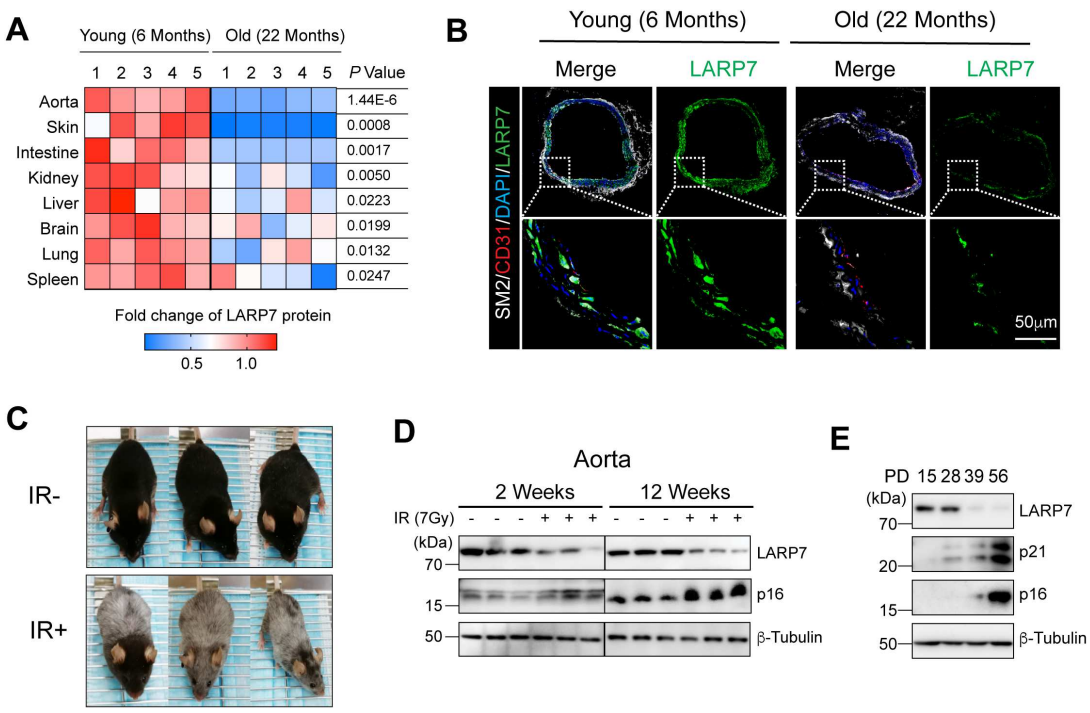

Figure 1

Figure 1. LARP7 was suppressed in aging and cellular senescence.

(A) Quantification of Western blotting showing LARP7 protein was downregulated in multiple organs of normally aging mice (22 months). All the young (6 months) and aging mice were in C57BL/6 background. Fold change represents the normalized LARP7 signal (LARP7/β-Tubulin) in aged mice relative to that in young mice. All the original blots were in the Supplemental Figure 1A. The heatmap were drawn by GENE-E matrix. n=5 mice in each group.

(B) LARP7 protein was markedly reduced in the aortic endothelium and smooth muscle of old mice as revealed by the immunofluorescence. CD31: a marker for endothelium; SM2: a marker for smooth muscle layer.

(C) The gross image of C57BL/6 mice 12 weeks after whole-body irradiation. The turning-grey coat color in irradiated mice indicated the premature ageing morphology.

(D) Western blotting showing IR induced the decline of LARP7 protein in the mouse aorta as early as two weeks. p16 upregulation indicated 7Gy whole-body irradiation induced the aortic senescence especially 12 weeks after IR. n=3.

(E) Western blotting showing LARP7 protein declined in IMR90 cells undergoing the replicative senescence. The replicative senescence was induced by doubling cells for 56 times, and implicated by the emerge of p21 and p16. PD denoted population doubling.

All quantifications in this figure were presented as Mean ± SD. Statistical analysis: unpaired two-tailed student's *t* test.

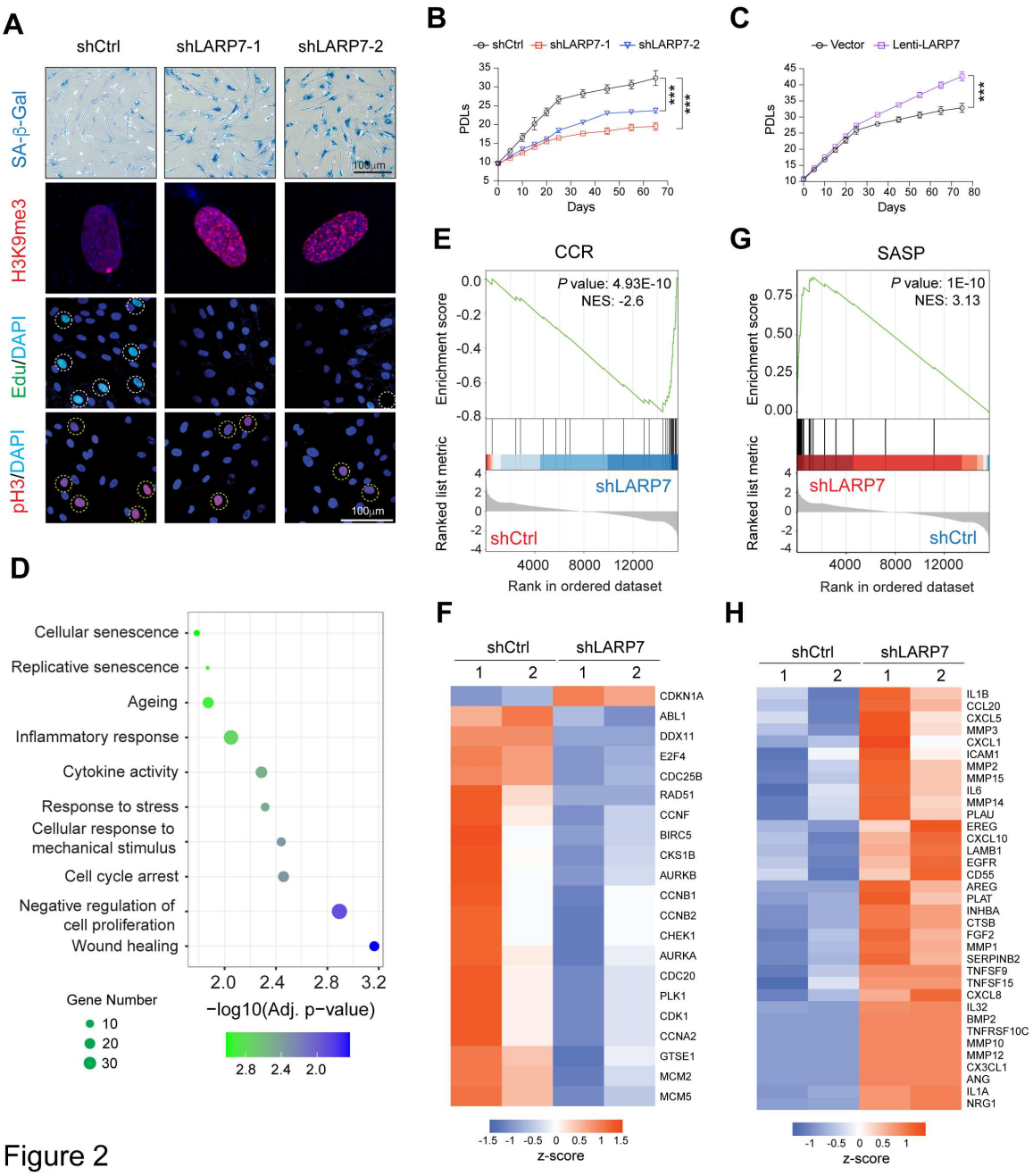

Figure 2

Figure 2. LARP7 depletion accelerated cellular senescence.

(A) Histological analysis showing LARP7-depleted IMR90 stable cell lines generated by two independent shRNA exhibited the increased senescence-associated β-Galactosidase activity (SA-β-Gal) and heterochromatin foci (SAHF), and decreased DNA replication (Edu) and cell division activity (pH3). SAHF were revealed by H3K9me3 immunofluorescent staining. Yellow dash circles indicated Edu or pH3 positive nuclei. The statistical quantifications were in Supplemental Figure 2B.

(B) Population doubling analysis showing LARP7-depleted IMR90 cells had declined proliferative potency. PDL denoted population doubling level.

(C) Population doubling analysis showing LARP7 overexpression increased the proliferative potency of IMR90 cells.

(D) GO analysis of DEG in LARP7-depleted IMR90 cells.

(E) Gene Set Enrichment Analysis (GSEA) illustrating the enrichment of cell cycle regulators in LARP7-depleted IMR90 cells. NES: normalized enrichment score. $P<0.05$ indicated significance.

(F) Heat map of altered cell cycle regulators in LARP7-depleted IMR90 cells.

(G) Gene Set Enrichment Analysis (GSEA) illustrating the enrichment of SASP genes in LARP7-depleted IMR90 cells. NES: normalized enrichment score. $P<0.05$ indicated significance.

(H) Heat map of altered cell cycle regulators in LARP7-depleted IMR90 cells.

All quantifications in this figure were presented as Mean ± SD. Statistical analysis: the PDL curves were analyzed by linear regression. ***: $P<0.001$.

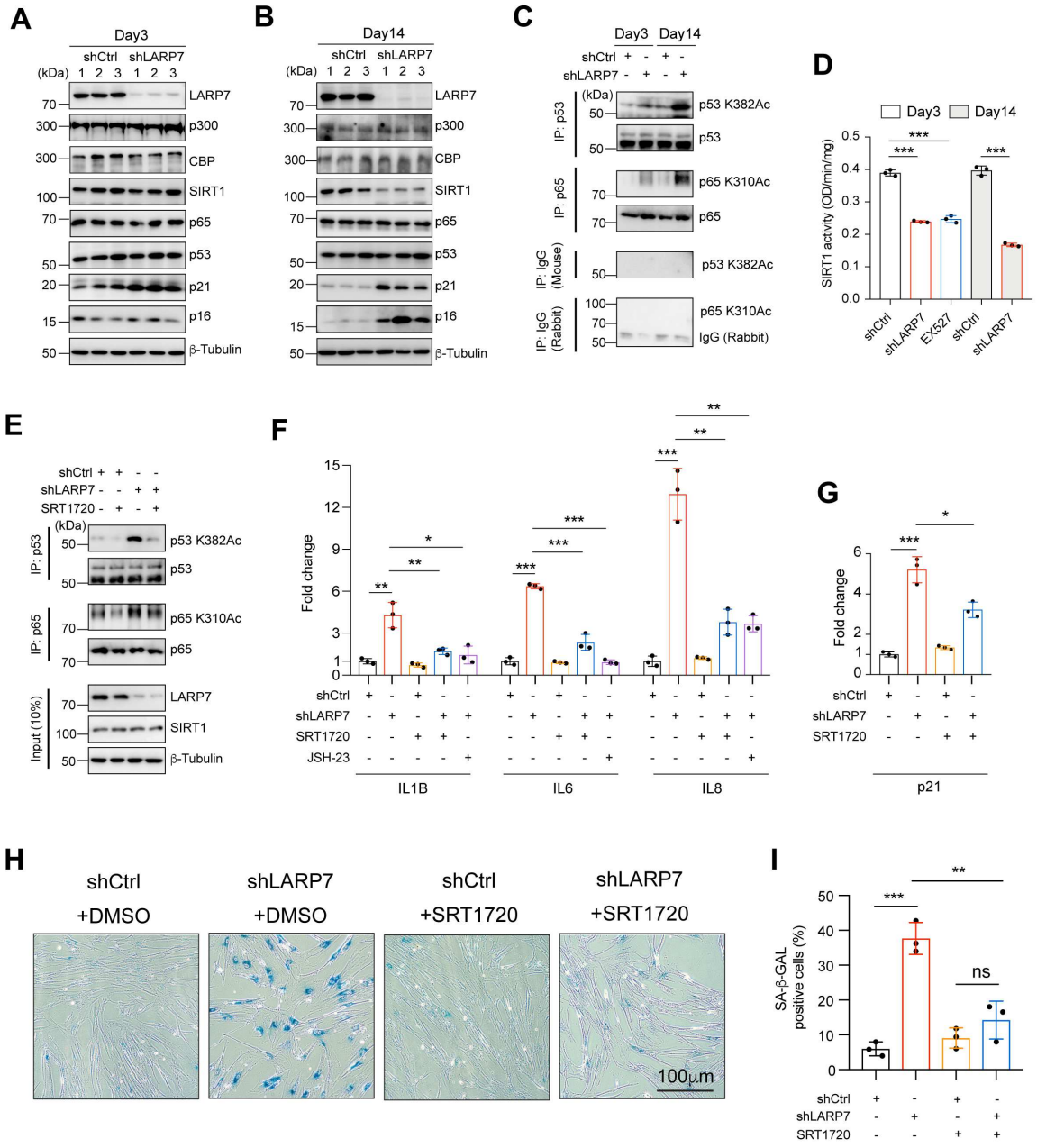

Figure 3

Figure 3. The declined SIRT1 deacetylase activity accounted for LARP7-induced **senescence.**

(A) Western blotting assessing the senescent regulators in IMR90 receiving LARP7 shRNA knockdown for 3 days.

(B) Western blotting assessing the senescent regulators in IMR90 receiving LARP7 shRNA knockdown for two weeks.

(C) LARP7 knockdown for 3 and 14 days in IMR90 cells increased the acetylation on specific lysine residues of p53 (K382) and p65 (K310). The acetylation of p53 (K382) and p65 (K310) were detected by acetylation-specific antibody after immunoprecipitated with p53 and p65

antibody. The control IgG (rabbit for p65 and mouse for p53) didn't pull down neither p53 or p65 indicating the specificity of immunoprecipitation.

(D) Knocking down LARP7 suppressed the SIRT1 deacetylase activity on both Day3 and 14. 10 μM EX527 inhibitor specific for SIRT1 was used as a positive control.

(E) The increased p53 and p65 acetylation upon LARP7 depletion were blocked by SIRT1-specific agonist SRT1720. shCtrl- or shLARP7-transfected IMR90 cells were treated with 1 μM SRT1720 for 12 hours and then subjected to immunoprecipitation.

(F) RT-qPCR showing SRT1720 abrogated the SASP gene activation. 2 μM JSH-23, the specific inhibitor for NF-κB, treated IMR90 cells for 48h, and was used as positive control. n=3.

(G) RT-qPCR showing SRT1720 abrogated p21 induction in LARP7-depleted IMR90 cells.

(H-I) SA-β-Gal staining demonstrated that SRT1720 effectively halted the LARP7 depletion-induced senescence. 1 μM SRT1720 were applied to IMR90 cells for 2 days before SA-β-Gal staining (H), and the percentage of SA-β-Gal positive cells were quantified (I). n=3 independent experiments.

All quantifications in this figure were presented as Mean ± SD. Statistical analysis: unpaired two-tailed student's *t* test. *: $P<0.05$, **: $P<0.01$, ***: $P<0.001$. ns: no significance.

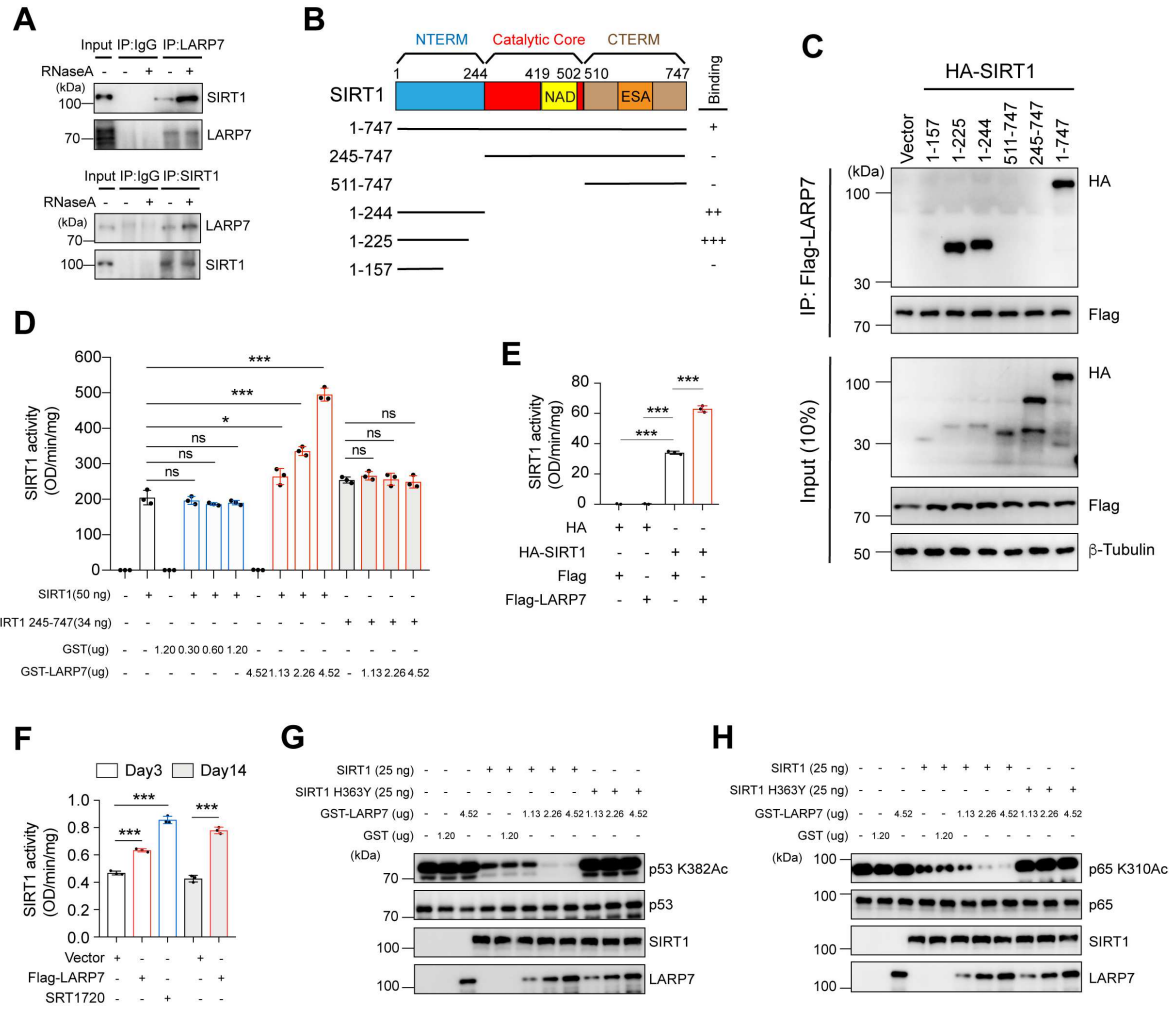

Figure 4

Figure 4. LARP7 enhanced SIRT1 deacetylase activity by directly interacting with its N-terminal activation domain.

(A) LARP7 interacted with SIRT1 in IMR90 cells as assessed by immunoprecipitation with LARP7 (Top) and reciprocal immunoprecipitation with SIRT1 (Bottom). The 5 μg/ml RNase A was subjected to nuclear protein lysis to remove 7SK RNA, and the results indicted SIRT1-LARP7 interaction is independent of 7SK RNA.

(B) Schematic diagram showing functional domains of SIRT1, domain deletions and binding affinity between LARP7 and SIRT1 domain deletions.

(C) Domain deletion assay in 293T cells indicated LARP7 interacted with SIRT1 N-Terminal domain (157-244).

(D) *In vitro* SIRT1 deacetylase activity assay showing LARP7 augmented SIRT1 activity in a dose-dependent mean, which required the N-Terminal allosteric activation domain of SIRT1. GST-LARP7, SIRT1 and SIRT1 (245-747) were expressed in E.Coli BL21 (Supplemental Figure 3D), and SIRT1 activity assay kit was used to measure SIRT1 deacetylase activity.

(E) *In vitro* SIRT1 activity assay demonstrated LARP7 enhanced the intracellular SIRT1 enzymatic activity. Flag-LARP7 and HA-SIRT1 were purified from 293T cells.

(F) LARP7 overexpression promoted SIRT1 activity *in vivo*. IMR90 cells were transfected with indicated constructs or treated with SRT1720 (1μM) for 12 h.

(G-H) *In vitro* deacetylation assay showing LARP7 enhanced SIRT1-mediated deacetylation of p53 and p65. The acetylated p53 (G) and p65 (H) were generated by reacting with histone acetyltransferase p300, and validated by p65 (K310Ac) and p53 (K382Ac) specific antibody (Supplemental Figure 3F, G).

All the data in this figure are plotted in Mean ± SD. Two-tailed Student's t test was used for the statistical analysis. Data reflecting three independent experiments. *: $P<0.05$, **: $P<0.01$, ***: $P<0.001$.

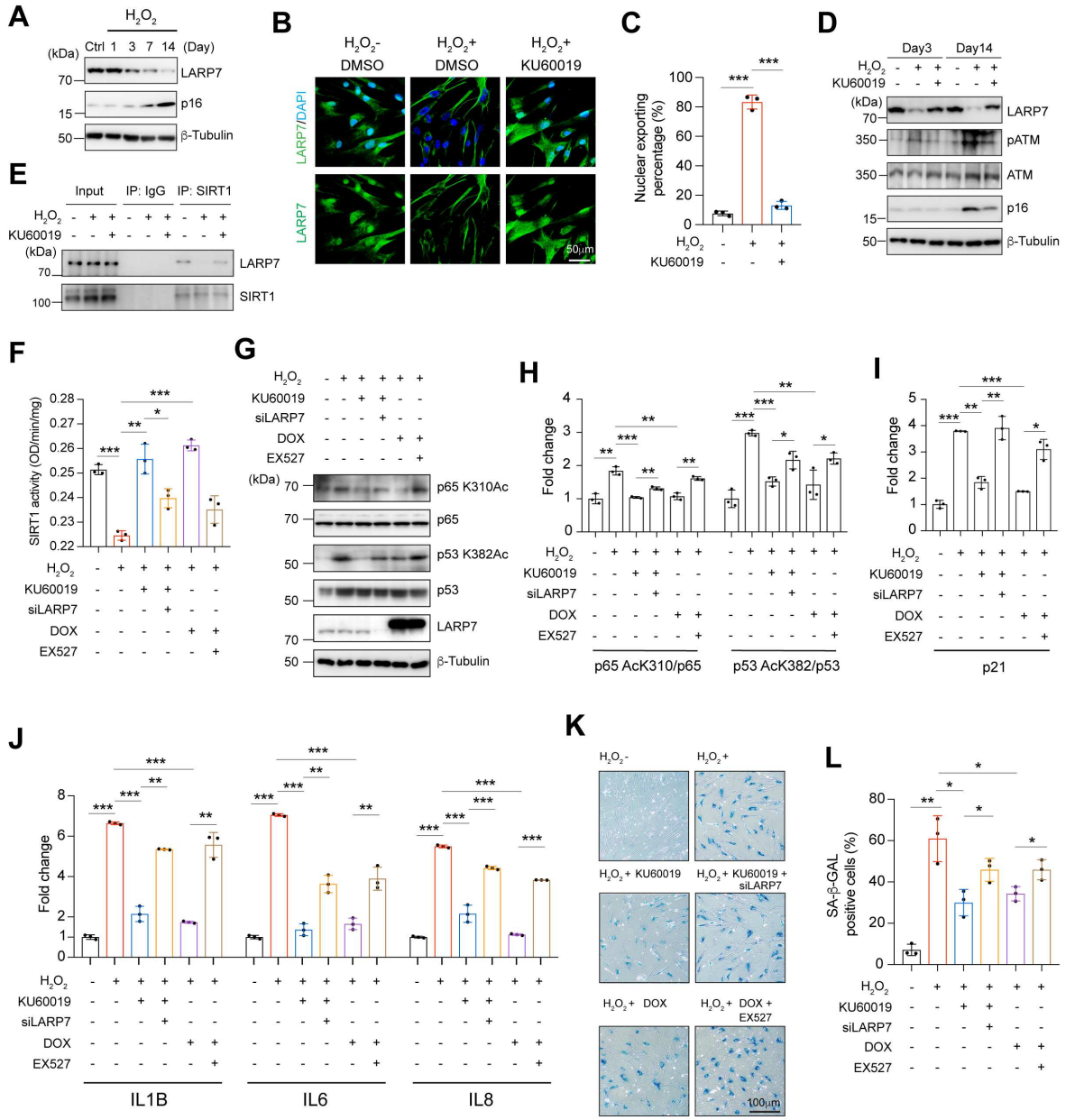

Figure 5

Figure 5. ATM-LARP7-SIRT1 axis mediated DDR-induced cellular senescence.

(A) Western blotting showing LARP7 was downregulated after H_2O_2 treatment. IMR90 cells were exposed to 100 μM H_2O_2 for 2 hours.

(B-C) Immunofluorescence staining showing LARP7 was shuttled out of nuclei upon H_2O_2 treatment and which was prevented by KU60019. Cells were stained with LARP7 specific antibody 6 h after H_2O_2 treatment (B), and the percentage of extranuclear exportation was calculated (C). n=3 independent experiments.

(D) ATM mediated LARP7 degradation induced by H_2O_2. ATM inhibitor KU60019 (10 μM) was pre-incubated with IMR90 cells 2 h before adding 100 μM H_2O_2.

(E) Immunoprecipitation illustrated that H_2O_2 disrupted LARP7-SIRT1 interaction in IMR90 cells, and which was reversed by ATM inhibition.

(F) SIRT1 activity assay in IMR90 cells showing H_2O_2 repressed SIRT1 activity, which was blocked by ATM inhibition or ectopic expression of LARP7. ATM inhibition reversed SIRT1 activity depending on LARP7 as revealed by siLARP7. IMR90 cells were treated with KU60019 (10 μM) or doxycycline (1 μg/ml, to induce LARP7) or EX527 (10 μM, a SIRT1 inhibitor).

(G-H) ATM inhibition or doxycycline-induced LARP7 overexpression abolished H_2O_2-induced p65 and p53 acetylation. IMR90 cells were pretreated with KU60019 (10μM) or doxycycline (1 μg/ml) or EX527 (10 μM), and then with 100 μM H_2O_2 for 2 hours. 24 hours after washing out H_2O_2, the cells were subjected to WB for testing (G) and the blots were quantified with image J (H). n=3 independent experiments.

(I-J) ATM inhibition or LARP7 overexpression abolished H_2O_2-induced p21 and SASP expression. p21 (I) and SASP (J) were measured with RT-qPCR 14 days after H_2O_2 treatment. n=3 independent experiments.

(K-L) SA-β-Gal staining showing KU60019 and LARP7 overexpression reversed the H_2O_2-induced cellular senescence. IMR90 cells were treated with KU60019 (10 μM) or doxycycline (1 μg/ml, to ectopically express LARP7) or EX527 (a SIRT1 inhibitor, 10 μM) for 14 days before subjected to SA-β-Gal staining and quantified with image J. n=3 assays.

All the data in this figure were plotted in Mean ± SD. Two-tailed Student's t test was used for the statistical analysis. *: $P<0.05$, **: $P<0.01$, ***: $P<0.001$.

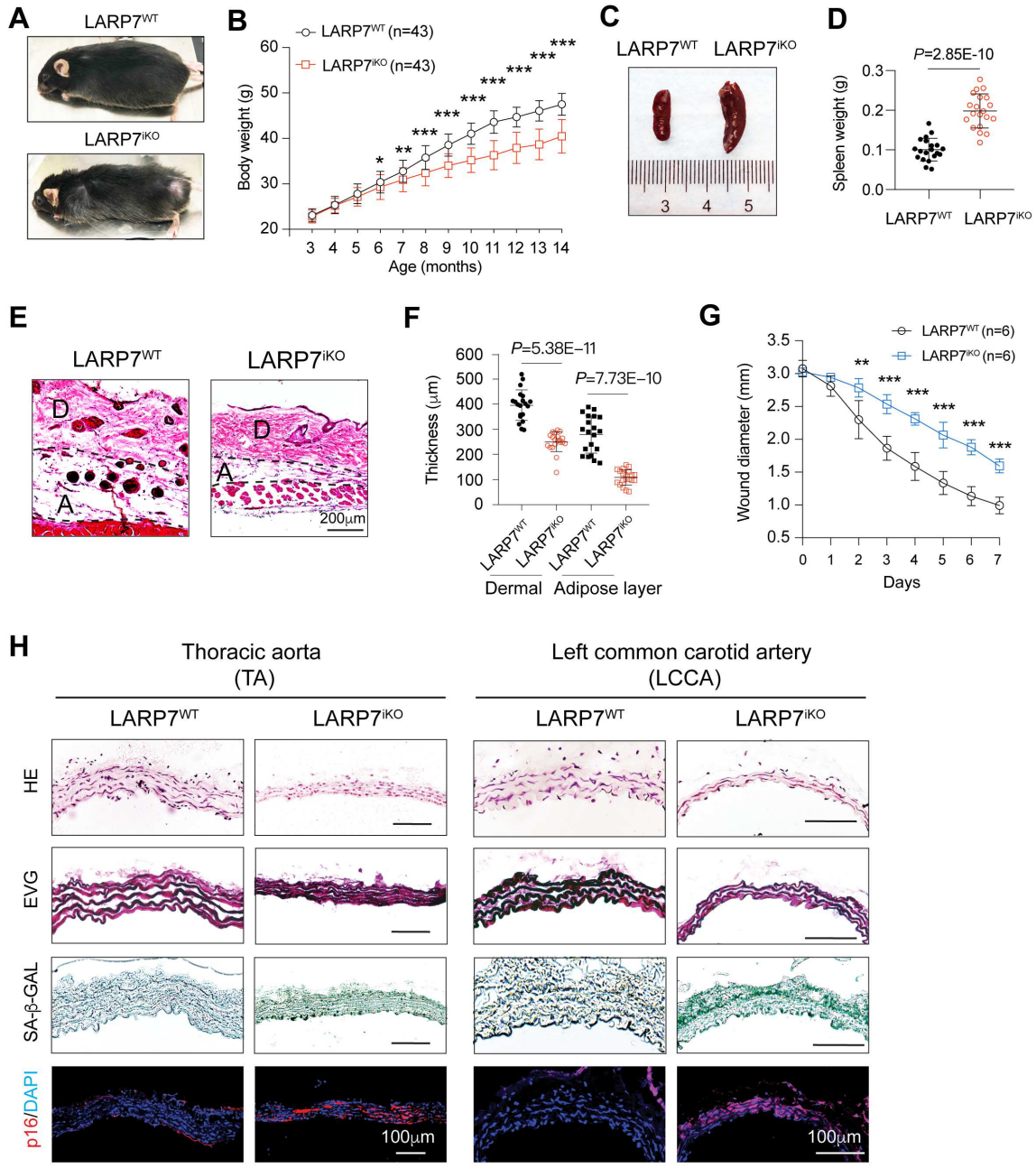

Figure 6

Figure 6. LARP7 deficiency induced the premature aging *in vivo*.

(A) Photographs of 14-month-old LARP7^{iKO} mice illustrating a premature aging phenotype comparing to wildtype littermates.

(B) Growth curves of LARP7^{iKO} mice and uninduced control mice. n=43 mice in each group.

(C) Representative figure of spleen of 14-month-old LARP7^{WT} and LARP7^{iKO} mice.

(D) Statistical analysis of spleen weight of 14-month-old LARP7^{WT} and LARP7^{iKO} mice.

(E) HE staining showing the age-related abnormalities in the skin of LARP7^{iKO} mice. A: subcutaneous adipose layer, D: dermis.

(F) Statistical analysis of the thickness of subcutaneous adipose and dermal layer. n=20 mice.

(G) Wound healing curves of 3-mm punch biopsy wounds in 14-month-old LARP7^{iKO} and LARP7^{WT} mice. n=6 mice.

(H) Vessel images (HE, EVG, SA-β-Gal and p16 staining) showing age-related phenotypes in the thoracic aorta and left common carotid artery of 14-month-old LARP7^{iKO} mice. TA: thoracic aorta, LCCA: left common carotid artery. EVG staining is to reveal the elastic fiber using Elastic stain kit.

All plot data were presented as Mean ± SD. The comparison of 6-month-old mice weight in 6B was using Mann-Whitney U test, the others were tested with two-tailed student's t test. *: $P<0.05$, **: $P<0.01$, ***: $P<0.001$.

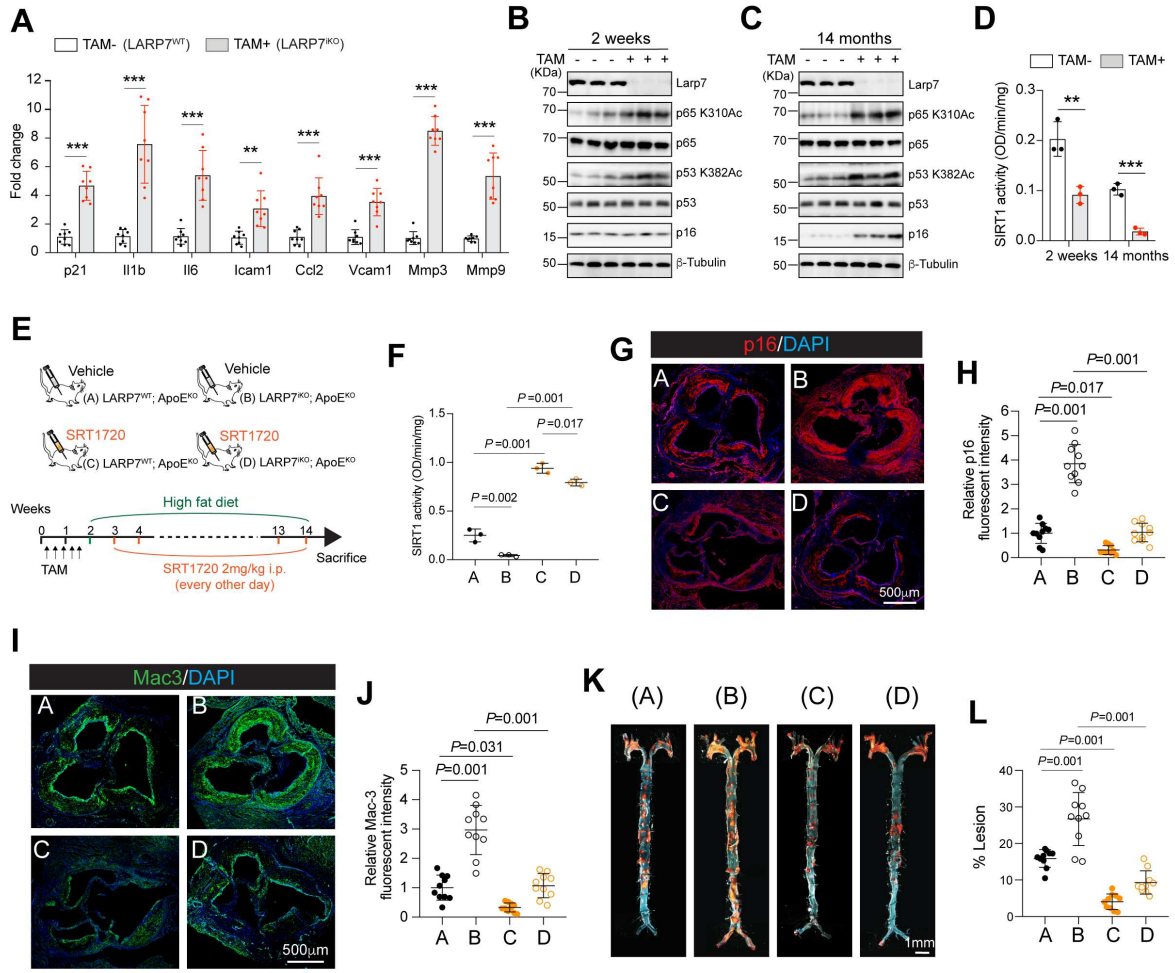

Figure 7

Figure 7. LARP7 deficiency accelerated vascular senescence and atherogenesis in ApoE^{KO} mice by attenuating SIRT1 deacetylase activity.

(A) SASP genes and p21 were upregulated in LARP7^{iKO} aortas 14 months after TAM induction. n=8 mice.

(B) Aortas of LARP7^{iKO} mice showing elevated acetylation of p65 and p53 after depletion of LARP7 for 2 weeks.

(C) Elevated acetylation of p65 and p53 in aorta after depletion of LARP7 for 14 months. p16 elevated significantly in LARP7-depleted aortas indicated accumulated senescence.

(D) LARP7 depletion significantly attenuated the SIRT1 activity in the aortas especially 14 months after induction. n=3 mice.

(E) The dose strategy of SRT1720 and HFD for LARP7^{WT}; ApoE^{KO} and LARP7^{iKO}; ApoE^{KO} mice. 50 mg/kg TAM were intraperitoneally injected every other day for 5 times to eliminate LARP7 before treating with SRT1720 and HFD. For SIRT1 activation, 2 mg/kg SRT1720 or vehicle solution (2% DMSO + 30% PEG300 + 1% Tween80) were intraperitoneally injected every other day for 3 months.

(F) SIRT1 activity assays illustrating SIRT1 deacetylase activity decreased in aortas of LARP7^{iKO}; ApoE^{KO} mice, and SRT1720 significantly elevated the SIRT1 activity in both LARP7^{WT}; ApoE^{KO} and LARP7^{iKO}; ApoE^{KO} mice aortas. n=3 aortas.
(G-H) p16 staining showing LARP7 depletion increased the senescent cells accumulation in the atherosclerotic lesion of ApoE^{KO} mice, but which was mitigated by SRT1720. n=10 aortas.
(I-J) Mac3 staining to unveil the infiltrated macrophages and inflammatory status in aortic roots. Representative staining images (I) and relative Mac3 fluorescent intensity (all versus ApoE^{KO} group A, J) were presented. n=10 aortas.
(K-L) LARP7 depletion increased the atherogenesis which was reversed by the treatment with SRT1720. The representative images of atherosclerosis lesions of aorta en face stained by oil red (K). The calculation of percentage of lesion area relative to total region (L). n=10 mice for each group.
All plots were presented as Mean ± SD, Figure 7D was tested with two-tailed student's t test, the rest plots were tested with one-way ANOVA followed by Tukey post-hoc test. P<0.05 indicated significance.

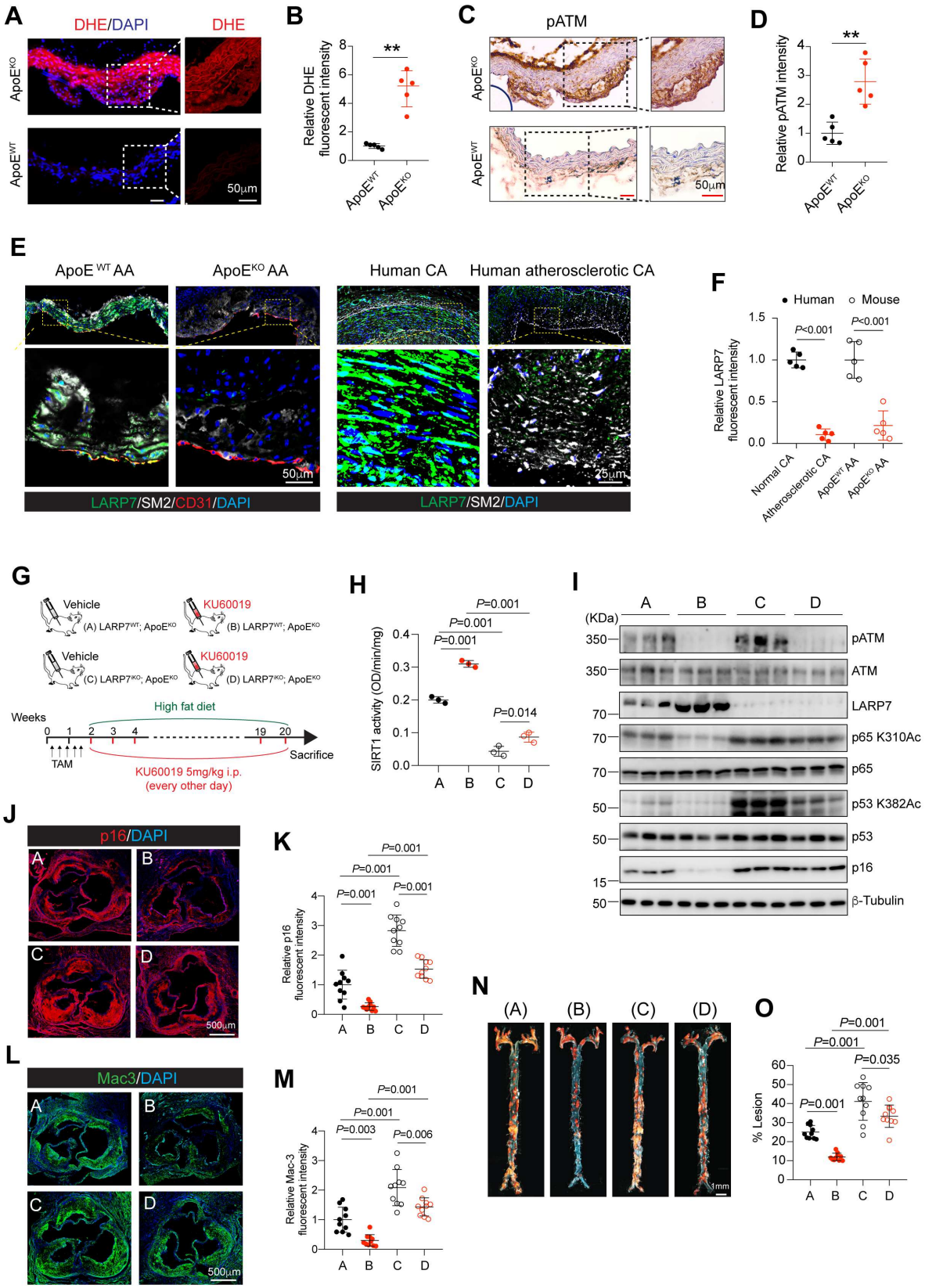
A
DHE/DAPI
DHE
ApoE^KO
ApoE^WT
50μm
B
Relative DHE fluorescent intensity
**
ApoE^WT
ApoE^KO
C
pATM
ApoE^KO
ApoE^WT
50μm
D
Relative pATM intensity
**
ApoE^WT
ApoE^KO
E
ApoE WT AA
ApoE KO AA
Human CA
Human atherosclerotic CA
50μm
25μm
LARP7/SM2/CD31/DAPI
LARP7/SM2/DAPI
F
Human
Mouse
Relative LARP7 fluorescent intensity
P<0.001
P<0.001
Normal CA
Atherosclerotic CA
ApoE^WT AA
ApoE^KO AA
G
Vehicle
(A) LARP7^WT; ApoE^KO
KU60019
(B) LARP7^WT; ApoE^KO
Vehicle
(C) LARP7^KO; ApoE^KO
KU60019
(D) LARP7^KO; ApoE^KO
High fat diet
Weeks
0 1 2 3 4 19 20
Sacrifice
TAM
KU60019 5mg/kg i.p.
(every other day)
H
SIRT1 activity (OD/min/mg)
P=0.001
P=0.001
P=0.001
P=0.014
A B C D
I
A B C D
(KDa)
350 pATM
350 ATM
70 LARP7
70 p65 K310Ac
70 p65
50 p53 K382Ac
50 p53
15 p16
50 β-Tubulin
J
p16/DAPI
A
B
C
D
500μm
K
Relative p16 fluorescent intensity
P=0.001
P=0.001
P=0.001
P=0.001
A B C D
L
Mac3/DAPI
A
B
C
D
500μm
M
Relative Mac-3 fluorescent intensity
P=0.001
P=0.001
P=0.003
P=0.006
A B C D
N
(A)
(B)
(C)
(D)
1mm
O
% Lesion
P=0.001
P=0.001
P=0.035
P=0.001
A B C D

Figure 8

Figure 8. ATM inhibition alleviated vascular senescence and atherogenesis.

(A-B) Dihydroethidium (DHE) staining illustrating elevated ROS in the atherogenic aorta. Freshly isolated aorta from $ApoE^{WT}$ and $ApoE^{KO}$ mice receiving HFD for 8 weeks were stained with DHE (A), and the staining density was quantified with ImageJ (B). n=5 aortas.

(C-D) Immunohistochemistry of phosphorylated ATM illustrated the hyperactivation of ATM pathway in atherogenic aorta. The aorta from $ApoE^{KO}$ mice receiving HFD for 2 months were applied for the pATM staining (C), and pATM intensity was quantified with ImageJ (D).

(E-F) Immunofluorescence staining showing LARP7 markedly declined in atherosclerotic lesions of arch aorta of $ApoE^{KO}$ mice and human coronary artery. The atherogenic arch aorta was isolated from $ApoE^{KO}$ mouse receiving HFD for 2 months. Human normal and atherogenic coronary arteries were obtained from the patients receiving heart transplantation. The LARP7 fluorescent intensity was calculated with ImageJ (F). CA: coronary artery; AA: arch aorta. n=5.

(G) The strategy for KU60019 administration. 5 mg/kg KU60019 were intraperitoneally injected to $LARP7^{WT}$; $ApoE^{KO}$ and $LARP7^{iKO}$; $ApoE^{KO}$ mice for 18 weeks.

(H) The SIRT1 activity in the aortas of $LARP7^{WT}$; $ApoE^{KO}$ and $LARP7^{iKO}$; $ApoE^{KO}$ mice treated with or without KU60019. n=3 aortas.

(I) Western blotting showing ATM inhibition decreased p16 expression and the acetylation of p53 and p65 in $LARP7^{WT}$; $ApoE^{KO}$ mice aorta, but which were comprised by the further knocking out LARP7. $LARP7^{WT}$; $ApoE^{KO}$ and $LARP7^{iKO}$; $ApoE^{KO}$ mice were fed with HFD for 18 weeks.

(J-K) p16 immunofluorescent staining showing KU60019 prevented the senescent cells accumulation in the aortic root, but which was compromised by knocking out LARP7. p16 fluorescent intensity from 10 aortic roots were calculated (K).

(L-M) Mac3 immunofluorescent staining of aortic root. The cryosection of aortic root was stained with Mac3 antibody (L), and the fluorescent intensity was calculated with ImageJ (M). n=10 mice.

(N-O) KU60019 markedly alleviated the atherogenesis of $LARP7^{WT}$; $ApoE^{KO}$ mice, but which was compromised by knockout of LARP7. The oil red staining of the aorta en face (N) was quantified as the percentage of lesion in total aortic area (O). n=10 aortas.

All plots were presented as Mean ± SD, Figure 8B, D and F was tested with two-tailed student's t test, the rest plots were tested with one-way ANOVA followed by Tukey post-hoc test. $P<0.05$ indicated significance.

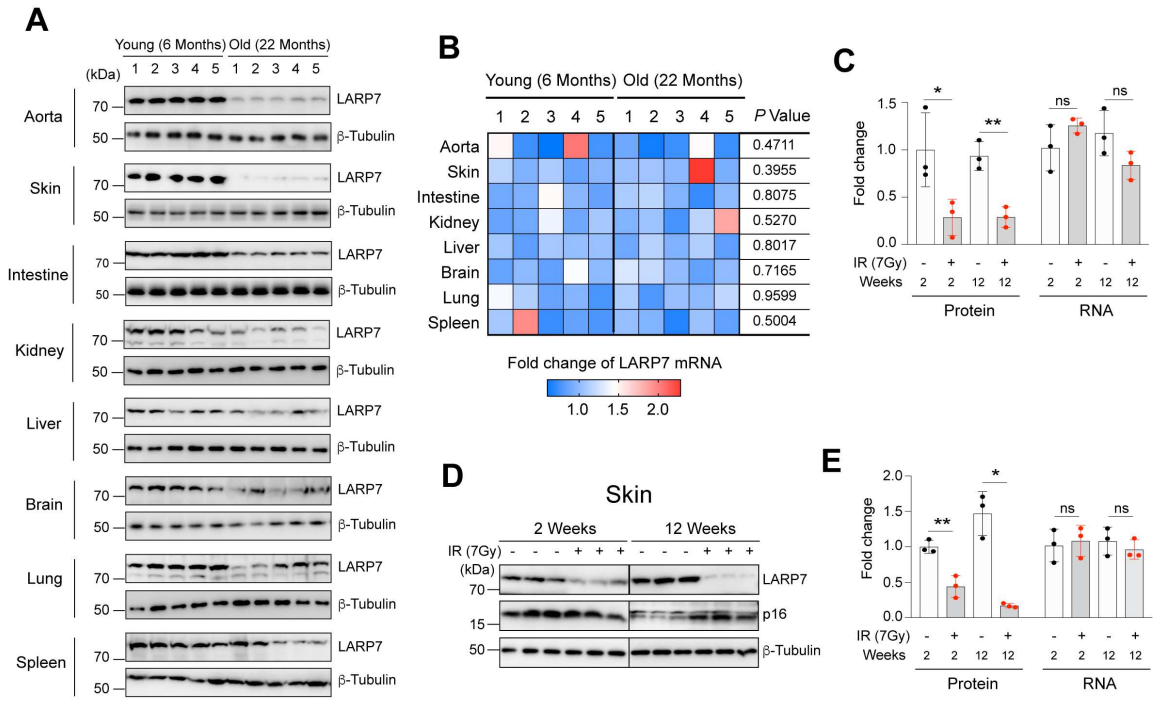

Supplemental Figure 1

Supplemental Figure 1. LARP7 was suppressed in aged mice.

(A) LARP7 protein level in diverse organs of aged mice (22 months) versus in young mice (6 months). LARP7 protein in aorta, skin, intestine, kidney, liver, brain, lung and spleen were measured with western blotting and quantified with the densitometric analysis in ImageJ. The quantifications were presented in Figure 1A.

(B) Quantification of RT-qPCR showing LARP7 mRNA is unchanged in aged mice comparing to the young mice. Similar to panel a, fold change represented the relative expression of LARP7 mRNA (LARP7/β-Tubulin) in aged mice comparing to that in young mice. n=5 mice in each group.

(C) Quantification of LARP7 protein and mRNA in the irradiated aorta according to Figure 1D.

(D-E) Assessment of LARP7 protein and mRNA in the irradiated skin. Protein was assessed with western blotting (D) and mRNA was assessed with RT-qPCR (E). n=3 tested mice.

All quantifications in this figure were presented as Mean ± SD. Statistical analysis: unpaired two-tailed student's *t* test. *: $P<0.05$, **: $P<0.01$, ns: no significance.

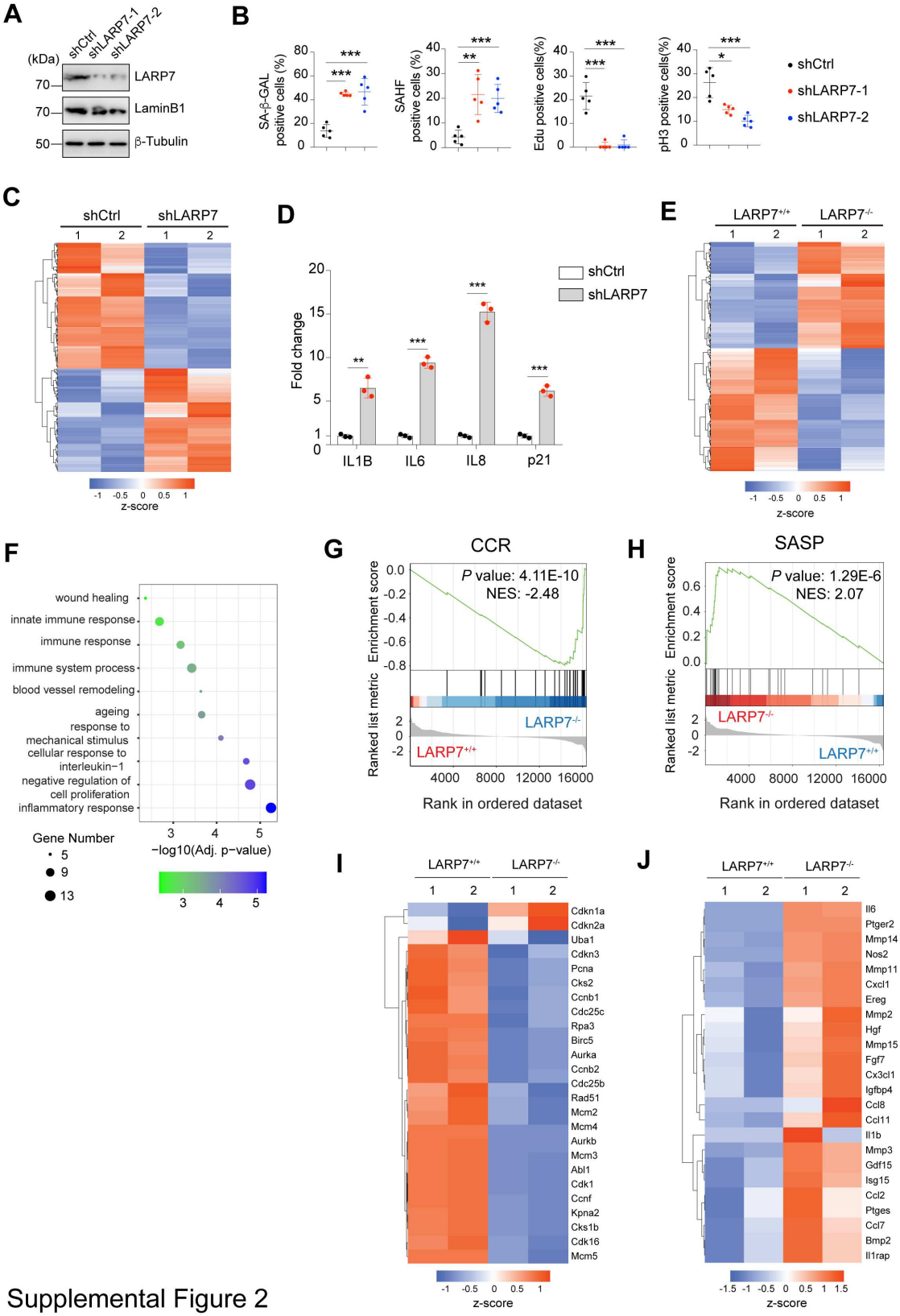

Supplemental Figure 2

Supplemental Figure 2. LARP7 deprivation induced cellular senescence.

(A) Western blotting showing LARP7 and LaminB1 were markedly suppressed in IMR90 cells stably transfected with two independent LARP7 shRNAs.

(B) Quantification of SA-β-Gal, SAHF, Edu and pH3 positive IMR90 cells corresponding to Figure 2A.

(C) Hierarchical heart map of DEGs in LARP7-depleted versus wildtype IMR90 cells.

(D) RT-qPCR validating the upregulation of three SASP genes (IL1B, IL6 and IL8) and p21 in LARP7-depleted IMR90 cells.

(E) Hierarchical Heart map of DEGs in LARP7-deleted versus wildtype MEFs.

(F) GO analysis of DEGs in MEFs.

(G) GESA analysis demonstrated the core cell cycle regulators (CCR) were preferentially altered by LARP7 deletion in MEFs.

(H) GESA analysis demonstrated SASP genes were preferentially affected by LARP7 deletion in MEFs.

(I) Heat map of cell cycle regulating genes upregulated in LARP7$^{-/-}$ MEFs.

(J) Heat map of SASP genes altered in LARP7$^{-/-}$ MEFs.

All quantifications in this figure were presented as Mean ± SD. Statistical analysis: unpaired two-tailed student's *t* test. **: $P<0.01$, ***: $P<0.001$.

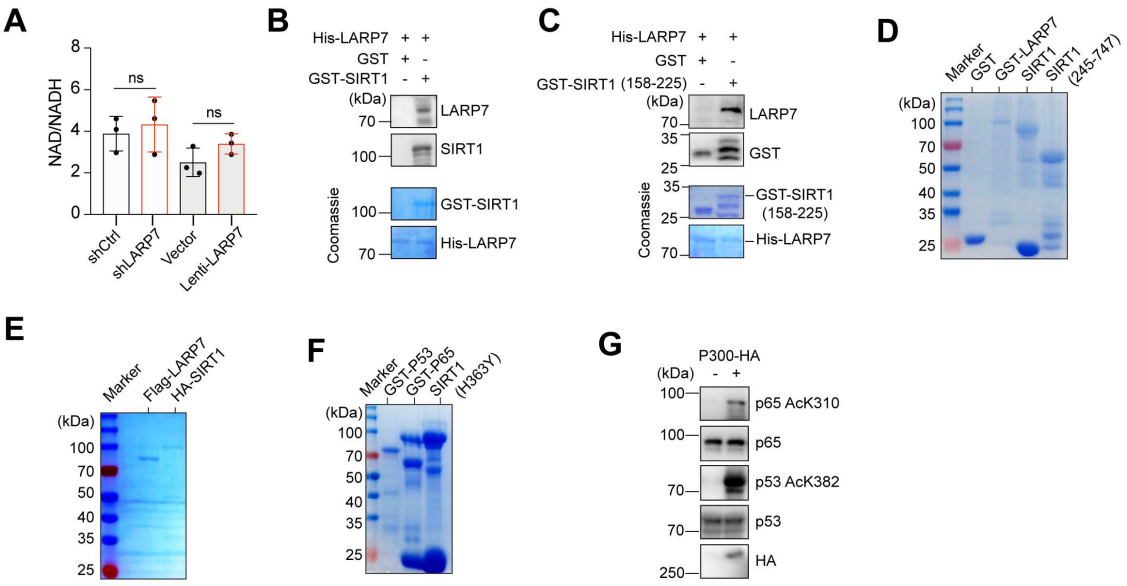

Supplemental Figure 3

Supplemental Figure 3. LARP7 enhanced SIRT1 deacetylase activity

(A) LARP7 knockdown or overexpression didn't alter the NAD^+/NADH ratio in IMR90 cells. NAD^+/NADH ratio was measured with NAD/NADH quantification kit. Data were presented as the mean ± SD. n=3 independent assays. Statistical analysis: unpaired two-tailed student's *t* test.

(B) GST pull-down assay demonstrated LARP7 directly interacted with SIRT1.

(C) GST pull-down assay showed a direct interaction between SIRT1 (158-225) and LARP7. GST-SIRT1 (158-225) and His-LARP7 were all purified from E. Coli.

(D) Gel validation of purified GST, GST-LARP7, SIRT1 and SIRT1 (245-747) protein from E. Coli corresponding to Figure 4D.

(E) Gel validation of Flag-LARP7 and HA-SIRT1 protein purified from KEK293T cells.

(F) Gel validation of recombinant GST-p53, GST-p65 and SIRT1 (H363Y) protein purified from E. Coli corresponding to Figure 4G, H.

(G) Western blotting evaluated the in *vitro* acetylated GST-p53 and GST-p65 protein. Purified GST-p53 or GST-p65 protein was incubated with HA-p300 purified from 293T cells for acetylation reaction, and then subjected to western blotting to validate the acetylation on p65 (K310Ac) and p53 (K382Ac) corresponding to Figure 4G, H.

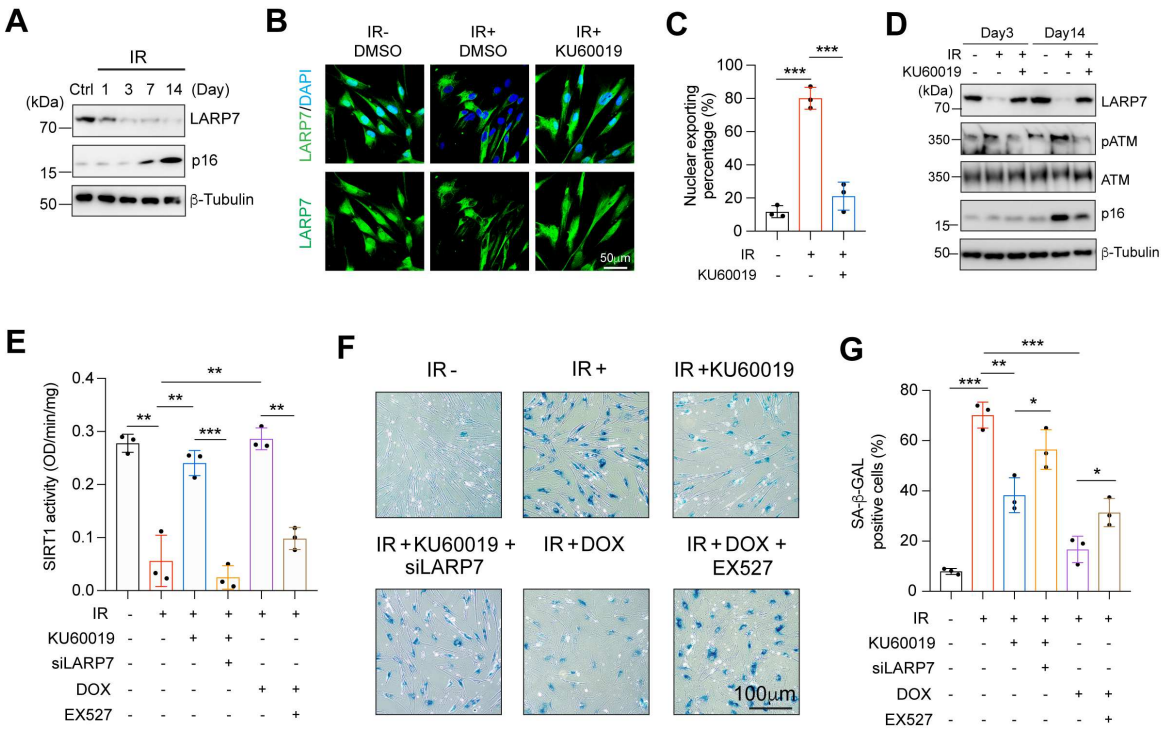

Supplemental Figure 4

Supplemental Figure 4. ATM-LARP7-SIRT1 axis mediated IR-induced senescence.

(A) Western blotting showing LARP7 was downregulated during IR treatment. IMR90 cells were exposed to X-ray (10 Gy).

(B-C) Immunofluorescence staining showing LARP7 was shuttled out of nuclei upon IR, and which was prevented by ATM inhibition. Cells were subjected to Immunofluorescence staining 6h after IR irradiation (B), and percentage of nuclear LARP7-exporting cells were calculated (C). n=3 experiments.

(D) ATM activation was required for IR-mediated LARP7 degradation. ATM inhibitor KU60019 (10 μM) was pre-incubated with IMR90 cells 2 h before IR irradiation.

(E) IR compromised SIRT1 activity in IMR90 cells, which was recovered by the KU60019 and LARP7 ectopic expression.

(F-G) IR induced IMR90 cellular senescence, and which was blocked by KU60019 and LARP7 overexpression. Irradiated IMR90 cells were treated with KU60019 (10 μM) or doxycycline (1 μg/ml), and the senescent cells was revealed by staining with SA-β-Gal (F). The percentage of SA-β-Gal positive cells was counted (G). n=3 assays.

All plotted data were in Mean ± SD, Two-tailed Student's t test was used for the statistical analysis. *: P<0.05, **: P<0.01, ***: P<0.001.

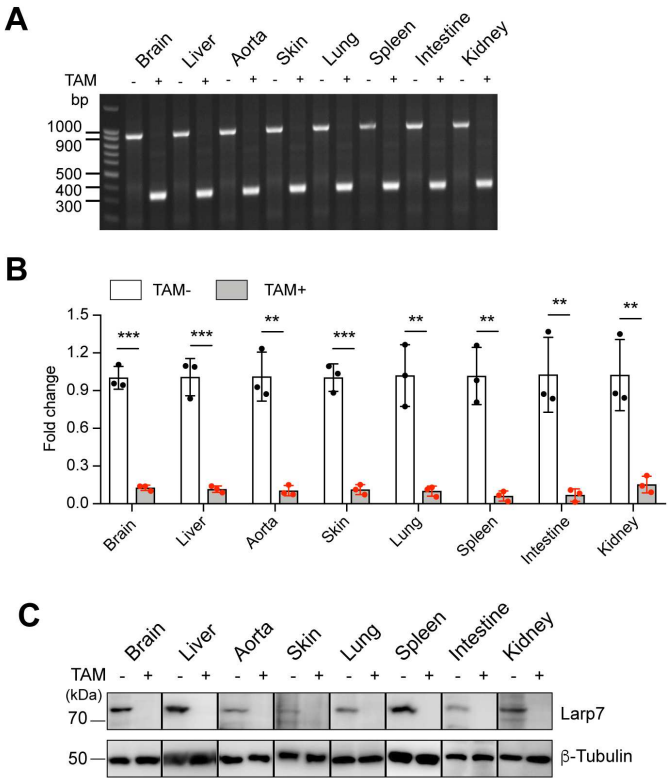

Supplemental Figure 5

Supplemental Figure 5. The characterization of LARP7^{iKO} mouse.

(A-C) Validation of LARP7 elimination on level of genome, mRNA and protein in multiple indicative organs of LARP7^{iKO} mice. *UBC*-Cre/ERT2; LARP7$^{f/f}$ mice were administrated intraperitoneally with TAM (50mg/kg) every other day for 5 times to knock out LARP7. The genomic deletion was tested by genomic PCR (A), mRNA by RT-qPCR (B) and protein by Western blotting (C) respectively. n=1-3 mice.

All plot data were presented as Mean ± SD, tested with two-tailed student's t test. **: P<0.01, ***: P<0.001.

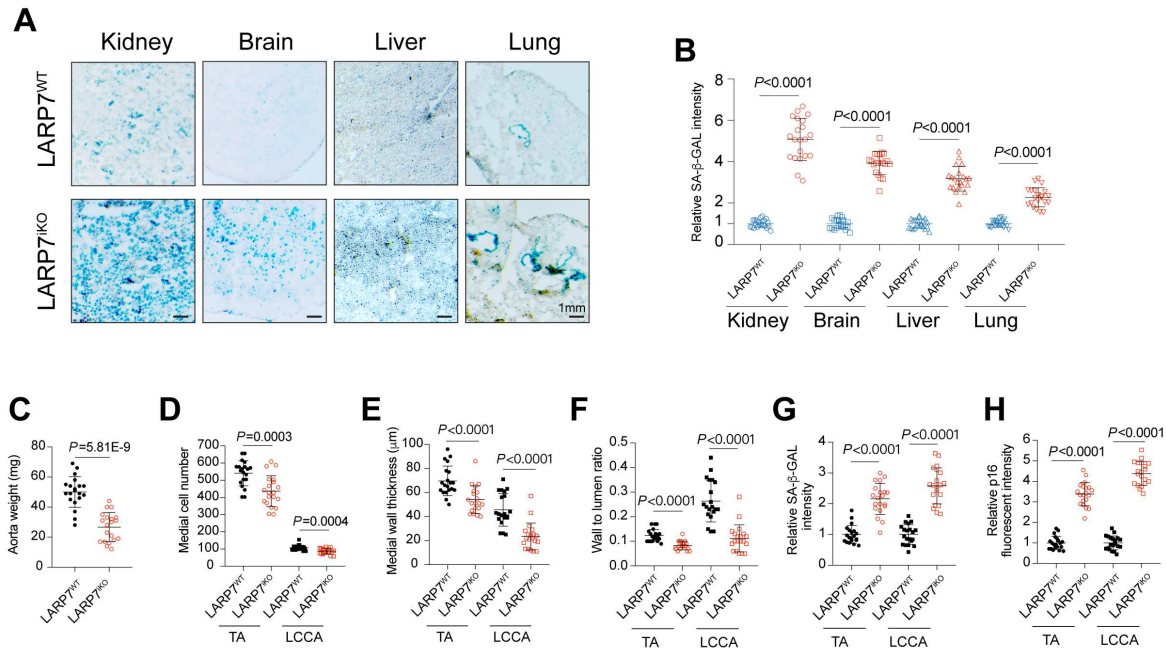

Supplemental Figure 6

Supplemental Figure 6. LARP7 depletion induced senescent cells accumulation in multiple organs.

(A) SA-β-Gal staining of kidney, brain, liver and lung sections in LARP7^{WT} and LARP7^{iKO} mice.

(B) Quantification of SA-β-Gal staining of kidney, brain, liver and lung sections in LARP7^{WT} and LARP7^{iKO} mice. n=20 mice in each group.

(C-H) Statistics analysis of aortic weight (C), cell number in tunica media (D), medial wall thickness (E), wall to lumen ratio (F), SA-β-Gal (G) and p16 staining (H) corresponding to Figure 6H. n=20 aortas.

All plot data were presented as Mean ± SD. SA-β-Gal quantification of brain in 6A, medial cell number of LCCA in 6D and wall thickness of TA and LCCA in 6E was using Mann-Whitney U test, the others were tested with two-tailed student's t test.

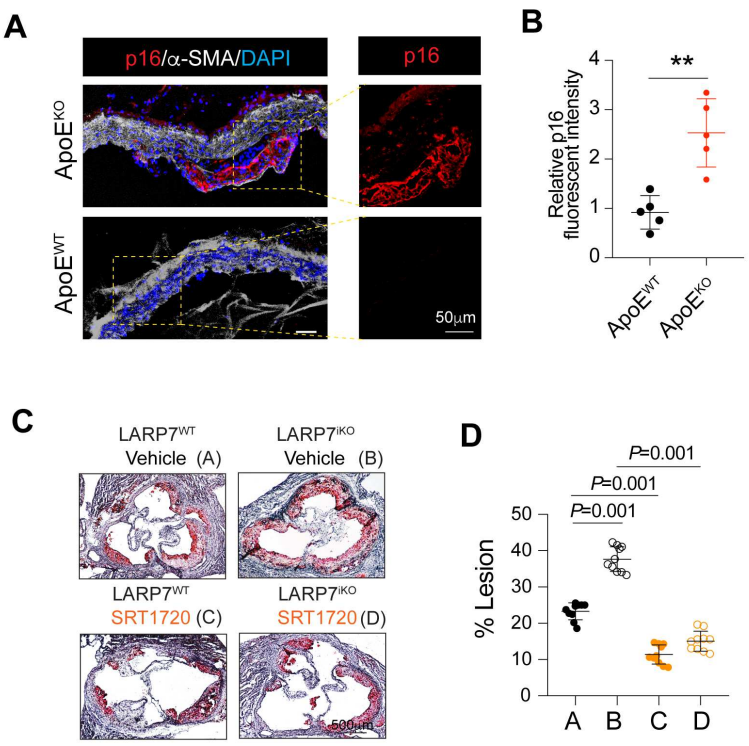

Supplemental Figure 7

Supplemental Figure 7. Senescent and oil red staining of atherogenic aorta.

(A-B) p16 staining showing increased senescent cells in the atherosclerotic plaques. Immunofluorescent staining was applied to reveal the senescent cells in arch aorta of ApoE^{KO} mice fed with HFD for 2 months, and p16 fluorescent intensity was calculated to reflect the senescent accumulation (right plot). n=5 aortas.

(C-D) Oil red staining of aortic root. The aortic root was cryosectioned and subjected to oil red staining (C), and the relative lesion area (%) was calculated and statistically analyzed (D). n=10 mice.

All plot data were presented as Mean ± SD, 6B was tested with two-tailed student's t test, 6D was tested with one-way ANOVA followed by Tukey post-hoc test **: P<0.01.

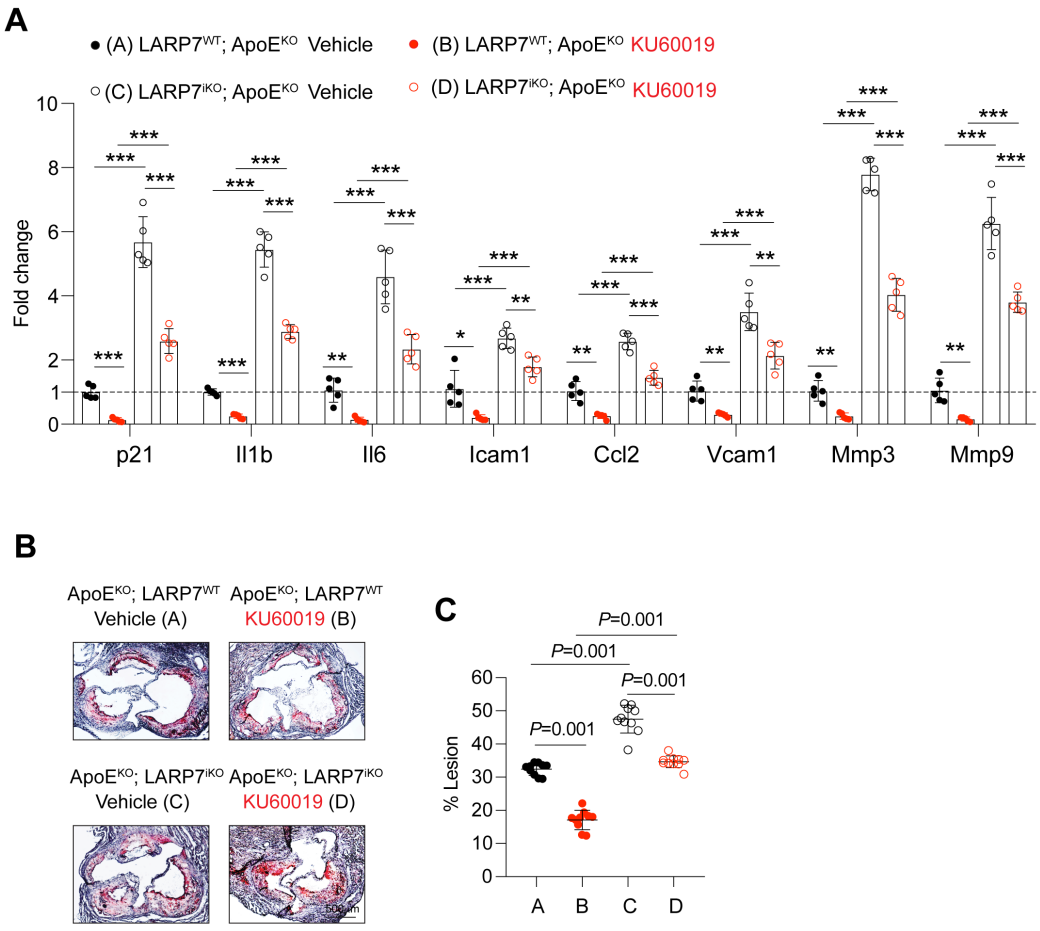

Supplemental Figure 8

Supplemental Figure 8. ATM-LARP7 axis aggravated vascular inflammation and atherogenesis.

(A) RT-qPCR showing p21 and SASP genes expression in aorta were markedly reduced by KU60019, and partially restored by further knocking out LARP7. n=5 aortas.

(B-C) Oil red staining of aortic root. The aortic root was subjected to oil red staining (B), and the relative lesion area (%) was calculated and statistically analyzed (C). n=10 mice.

All plots were presented as Mean ± SD, 8A and 8C were tested with one-way ANOVA followed by Tukey post-hoc test. $P<0.05$ indicated significance. *: $P<0.05$, **: $P<0.01$, ***: $P<0.001$.

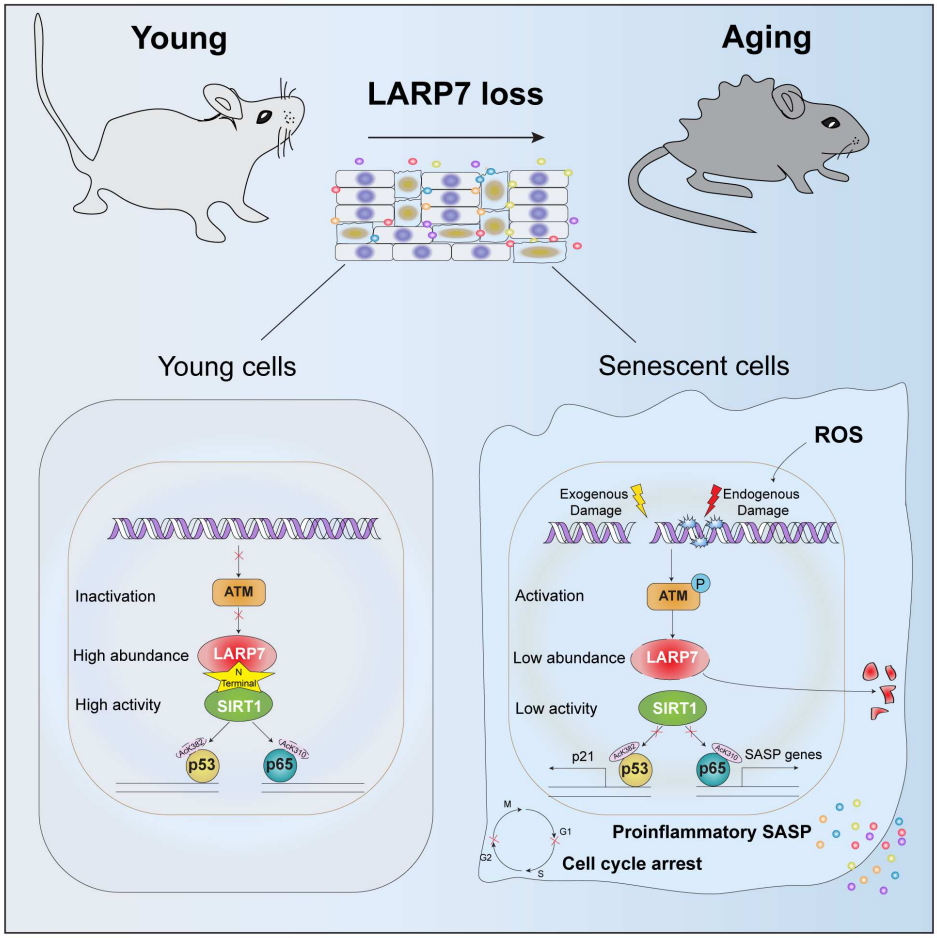

Supplemental Figure 9

Supplemental Figure 9. The working model of ATM-LARP7-SIRT1-P53/P65 axis in young and senescent cell.

References

1 Lopez-Otin, C., Blasco, M. A., Partridge, L., Serrano, M. & Kroemer, G. The hallmarks of aging. *Cell* **153**, 1194-1217, doi:10.1016/j.cell.2013.05.039 (2013).

2 Munoz-Espin, D. & Serrano, M. Cellular senescence: from physiology to pathology. *Nat Rev Mol Cell Biol* **15**, 482-496, doi:10.1038/nrm3823 (2014).

3 Gorgoulis, V. *et al.* Cellular Senescence: Defining a Path Forward. *Cell* **179**, 813-827, doi:10.1016/j.cell.2019.10.005 (2019).

4 Salama, R., Sadaie, M., Hoare, M. & Narita, M. Cellular senescence and its effector programs. *Genes & Development* **28**, 99-114, doi:10.1101/gad.235184.113 (2014).

5 Hayflick, L. & Moorhead, P. S. The serial cultivation of human diploid cell strains. *Exp Cell Res* **25**, 585-621, doi:10.1016/0014-4827(61)90192-6 (1961).

6 Hernandez-Segura, A., Nehme, J. & Demaria, M. Hallmarks of Cellular Senescence. *Trends Cell Biol* **28**, 436-453, doi:10.1016/j.tcb.2018.02.001 (2018).

7 Rodier, F. *et al.* Persistent DNA damage signalling triggers senescence-associated inflammatory cytokine secretion. *Nat Cell Biol* **11**, 973-979, doi:10.1038/ncb1909 (2009).

8 Baker, D. J. *et al.* Naturally occurring p16(Ink4a)-positive cells shorten healthy lifespan. *Nature* **530**, 184-189, doi:10.1038/nature16932 (2016).

9 Childs, B. G. *et al.* Senescent intimal foam cells are deleterious at all stages of atherosclerosis. *Science* **354**, 472-477 (2016).

10 Jacobs, J. J., Kieboom, K., Marino, S., DePinho, R. A. & van Lohuizen, M. The oncogene and Polycomb-group gene bmi-1 regulates cell proliferation and senescence through the ink4a locus. *Nature* **397**, 164-168, doi:10.1038/16476 (1999).

11 Wu, Z. H., Shi, Y., Tibbetts, R. S. & Miyamoto, S. Molecular linkage between the kinase ATM and NF-kappaB signaling in response to genotoxic stimuli. *Science* **311**, 1141-1146, doi:10.1126/science.1121513 (2006).

12 Kang, C. *et al.* The DNA damage response induces inflammation and senescence by inhibiting autophagy of GATA4. *Science* **349**, aaa5612, doi:10.1126/science.aaa5612 (2015).

13 Krueger, B. J. *et al.* LARP7 is a stable component of the 7SK snRNP while P-TEFb, HEXIM1 and hnRNP A1 are reversibly associated. *Nucleic Acids Res* **36**, 2219-2229, doi:10.1093/nar/gkn061 (2008).

14 Ahmed, K. M. & Li, J. J. NF-kappa B-mediated adaptive resistance to ionizing radiation. *Free Radic Biol Med* **44**, 1-13, doi:10.1016/j.freeradbiomed.2007.09.022 (2008).

15 Holohan, B. *et al.* Impaired telomere maintenance in Alazami syndrome patients with LARP7 deficiency. *BMC Genomics* **17**, 749, doi:10.1186/s12864-016-3093-4 (2016).

16 Alazami, A. M. *et al.* Loss of function mutation in LARP7, chaperone of 7SK ncRNA, causes a syndrome of facial dysmorphism, intellectual disability, and primordial dwarfism. *Hum Mutat* **33**, 1429-1434, doi:10.1002/humu.22175 (2012).

17 Dateki, S. *et al.* Novel compound heterozygous variants in the LARP7 gene in a patient with Alazami syndrome. *Hum Genome Var* **5**, 18014, doi:10.1038/hgv.2018.14 (2018).

18 Le, O. N. *et al.* Ionizing radiation-induced long-term expression of senescence markers in mice is independent of p53 and immune status. *Aging Cell* **9**, 398-409, doi:10.1111/j.1474-9726.2010.00567.x (2010).

19 Chang, J. *et al.* Clearance of senescent cells by ABT263 rejuvenates aged hematopoietic stem cells in mice. *Nat Med* **22**, 78-83, doi:10.1038/nm.4010 (2016).

20 Freund, A., Laberge, R. M., Demaria, M. & Campisi, J. Lamin B1 loss is a senescence-associated biomarker. *Mol Biol Cell* **23**, 2066-2075, doi:10.1091/mbc.E11-10-0884 (2012).

21 Wafik S. El-Deiry, T. T., Victor E. Velculescu, Daniel B. Levy, Ramon Parsons, Jeffrey M. Trent, David Lin, W. Edward Mercer, Kenneth W. Kinzler, and Bert Vogelstein. WAF1, a Potential Mediator of p53 Tumor Suppression. *Cell* **75**, 817-825 (1993).

22 Chien, Y. *et al.* Control of the senescence-associated secretory phenotype by NF-kappaB promotes senescence and enhances chemosensitivity. *Genes Dev* **25**, 2125-2136, doi:10.1101/gad.17276711 (2011).

23 Barlev, N. A. *et al.* Acetylation of p53 activates transcription through recruitment of coactivators/histone acetyltransferases. *Mol Cell* **8**, 1243-1254, doi:10.1016/s1097-2765(01)00414-2 (2001).

24 Chen, L. F. *et al.* NF-kappaB RelA phosphorylation regulates RelA acetylation. *Mol Cell Biol* **25**, 7966-7975, doi:10.1128/MCB.25.18.7966-7975.2005 (2005).

25 Akihiro Ito, C.-H. L., Xuan Zhao, Shin'ichi Saito, Maria H.Hamilton, Ettore Appella and Tso-Pang Yao. p300/CBP-mediated p53 acetylation is commonly induced by p53-activating agents and inhibited by MDM2. *The EMBO Journal* **20**, 1331-1340 (2001).

26 Yi, J. & Luo, J. SIRT1 and p53, effect on cancer, senescence and beyond. *Biochim Biophys Acta* **1804**, 1684-1689, doi:10.1016/j.bbapap.2010.05.002 (2010).

27 Yeung, F. *et al.* Modulation of NF-kappaB-dependent transcription and cell survival by the SIRT1 deacetylase. *EMBO J* **23**, 2369-2380, doi:10.1038/sj.emboj.7600244 (2004).

28 Lin-feng Chen, Y. M. a. W. C. G. Acetylation of RelA at discrete sites regulates distinct nuclear functions of NF-kB. *The EMBO Journal* **21**, 6539-6548 (2002).

29 Kim, E. J., Kho, J. H., Kang, M. R. & Um, S. J. Active regulator of SIRT1 cooperates with SIRT1 and facilitates suppression of p53 activity. *Mol Cell* **28**, 277-290, doi:10.1016/j.molcel.2007.08.030 (2007).

30 Jing Zhao, L. Z., Aiping Lu, Yingchao Han, Debora Colangelo, Christina Bukata, Alex Scibetta, Matthew J. Yousefzadeh, Xuesen Li, Aditi U. Gurkar, Sara J. McGowan, Luise Angelini, Ryan O'Kelly, Hongshuai Li, Lana Corbo, Tokio Sano, Heather Nick, Enrico Pola, Smitha P.S. Pilla, Warren C. Ladiges, Nam Vo, Johnny Huard, Laura J. Niedernhofer, Paul D. Robbins. ATM is a key driver of NF-κB-dependent DNA-damage-induced senescence, stem cell dysfunction and aging. *Aging* **12**, 4688-4710 (2020).

31 Zannini, L., Buscemi, G., Kim, J. E., Fontanella, E. & Delia, D. DBC1 phosphorylation by ATM/ATR inhibits SIRT1 deacetylase in response to DNA damage. *J Mol Cell Biol* **4**, 294-303, doi:10.1093/jmcb/mjs035 (2012).

32 Yuan, J., Luo, K., Liu, T. & Lou, Z. Regulation of SIRT1 activity by genotoxic stress. *Genes Dev* **26**, 791-796, doi:10.1101/gad.188482.112 (2012).

33 Ruzankina, Y. *et al.* Deletion of the developmentally essential gene ATR in adult mice leads to age-related phenotypes and stem cell loss. *Cell Stem Cell* **1**, 113-126, doi:10.1016/j.stem.2007.03.002 (2007).

34 Jani, B. & Rajkumar, C. Ageing and vascular ageing. *Postgrad Med J* **82**, 357-362, doi:10.1136/pgmj.2005.036053 (2006).

35 Wang, J. C. & Bennett, M. Aging and atherosclerosis: mechanisms, functional consequences, and potential therapeutics for cellular senescence. *Circ Res* **111**, 245-259, doi:10.1161/CIRCRESAHA.111.261388 (2012).

36 Ungvari, Z., Tarantini, S., Donato, A. J., Galvan, V. & Csiszar, A. Mechanisms of Vascular Aging. *Circ Res* **123**, 849-867, doi:10.1161/CIRCRESAHA.118.311378 (2018).

37 Childs, B. G. *et al.* Senescent intimal foam cells are deleterious at all stages of atherosclerosis. *Science* **354**, 472-477, doi:10.1126/science.aaf6659 (2016).

38 Ferrucci, L. & Fabbri, E. Inflammageing: chronic inflammation in ageing, cardiovascular disease, and frailty. *Nat Rev Cardiol* **15**, 505-522, doi:10.1038/s41569-018-0064-2 (2018).
39 Yutaka Nakashima, A. S. P., Elaine W. Raines, Jan L. Breslow, Russell Ross. ApoE-deficient mice develop lesions of all phases of atherosclerosis throughout the arterial tree. *Arteriosclerosis, Thrombosis, and Vascular Biology* **14**, 133-140 (1994).
40 Matthews, C. *et al.* Vascular smooth muscle cells undergo telomere-based senescence in human atherosclerosis: effects of telomerase and oxidative stress. *Circ Res* **99**, 156-164 (2006).
41 Mahmoudi, M. *et al.* Statins use a novel Nijmegen breakage syndrome-1-dependent pathway to accelerate DNA repair in vascular smooth muscle cells. *Circ Res* **103**, 717-725, doi:10.1161/CIRCRESAHA.108.182899 (2008).
42 Zhuang, T. *et al.* Endothelial Foxp1 Suppresses Atherosclerosis via Modulation of Nlrp3 Inflammasome Activation. *Circ Res* **125**, 590-605, doi:10.1161/CIRCRESAHA.118.314402 (2019).
43 Sinclair, D. A. & Guarente, L. Extrachromosomal rDNA circles--a cause of aging in yeast. *Cell* **91**, 1033-1042, doi:10.1016/s0092-8674(00)80493-6 (1997).
44 Kennedy, B. K. *et al.* Redistribution of silencing proteins from telomeres to the nucleolus is associated with extension of life span in S. cerevisiae. *Cell* **89**, 381-391, doi:10.1016/s0092-8674(00)80219-6 (1997).
45 Banks, A. S. *et al.* SirT1 gain of function increases energy efficiency and prevents diabetes in mice. *Cell Metab* **8**, 333-341, doi:10.1016/j.cmet.2008.08.014 (2008).
46 Haigis, M. C. & Sinclair, D. A. Mammalian sirtuins: biological insights and disease relevance. *Annu Rev Pathol* **5**, 253-295, doi:10.1146/annurev.pathol.4.110807.092250 (2010).
47 Zhang, F. *et al.* L ARP7 Is a BRCA1 Ubiquitinase Substrate and Regulates Genome Stability and Tumorigenesis. *Cell Rep* **32**, 107974, doi:10.1016/j.celrep.2020.107974 (2020).
48 Banerjee, S. *et al.* Loss of C/EBPδ Exacerbates Radiation-Induced Cognitive Decline in Aged Mice due to Impaired Oxidative Stress Response. *International Journal of Molecular Sciences* **20**, doi:10.3390/ijms20040885 (2019).

Figures

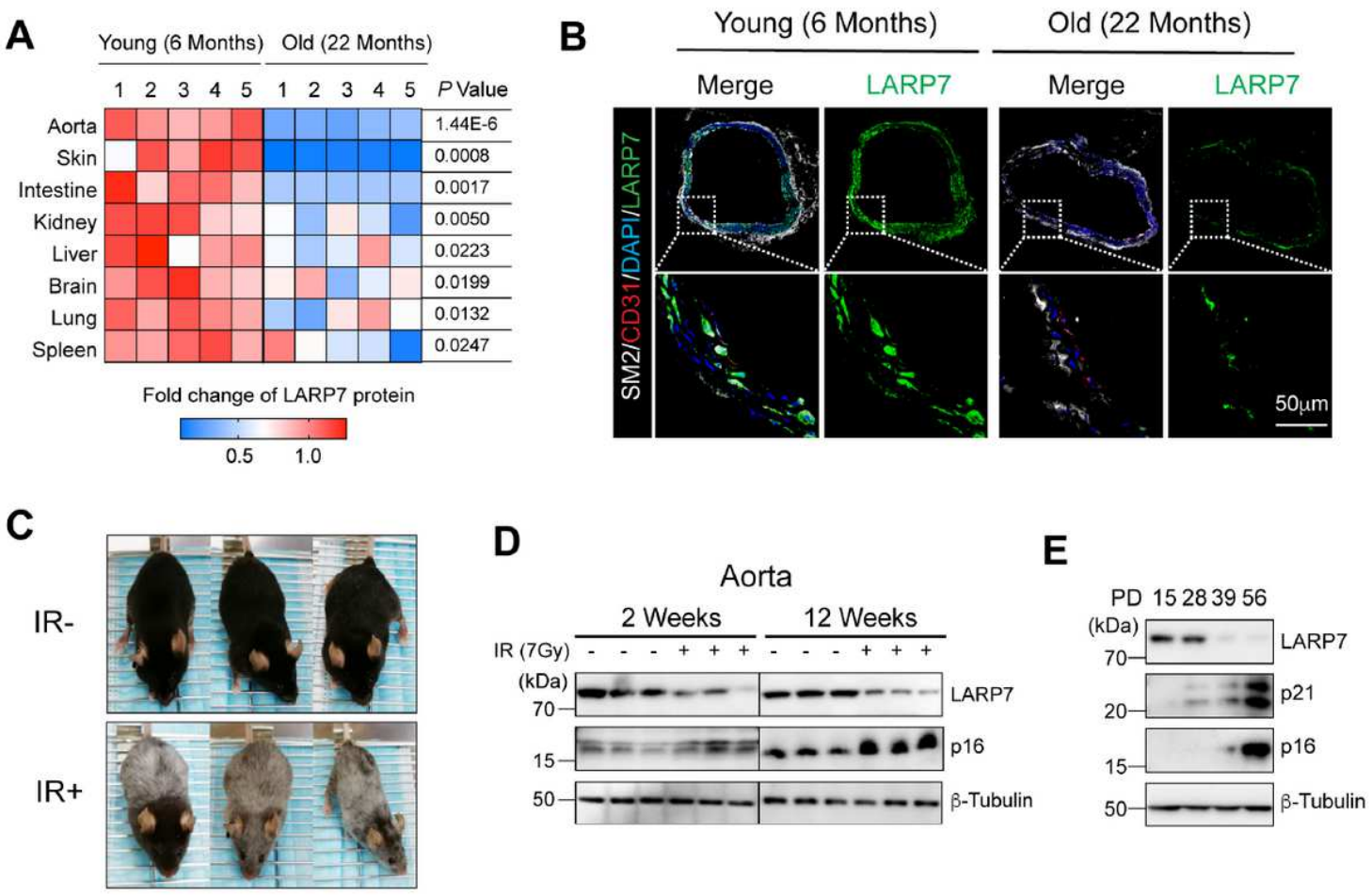

Figure 1

LARP7 was suppressed in aging and cellular senescence. (A) Quantification of Western blotting showing LARP7 protein was downregulated in multiple organs of normally aging mice (22 months). All the young (6 months) and aging mice were in C57BL/6 background. Fold change represents the normalized LARP7 signal (LARP7/b- Tubulin) in aged mice relative to that in young mice. All the original blots were in the Supplemental Figure 1A. The heatmap were drawn by GENE-E matrix. n=5 mice in each group. (B) LARP7 protein was markedly reduced in the aortic endothelium and smooth muscle of old mice as revealed by the immunofluorescence. CD31: a marker for endothelium; SM2: a marker for smooth muscle layer. (C) The gross image of C57BL/6 mice 12 weeks after whole-body irradiation. The turning-grey coat color in irradiated mice indicated the premature ageing morphology. (D) Western blotting showing IR induced the decline of LARP7 protein in the mouse aorta as early as two weeks. p16 upregulation indicated 7Gy whole-body irradiation induced the aortic senescence especially 12 weeks after IR. n=3. (E) Western blotting showing LARP7 protein declined in IMR90 cells undergoing the replicative senescence. The replicative senescence was induced by doubling cells for 56 times, and implicated by the emerge of p21 and p16. PD denoted population doubling. All quantifications in this figure were presented as Mean ± SD. Statistical analysis: unpaired two-tailed student's t test.

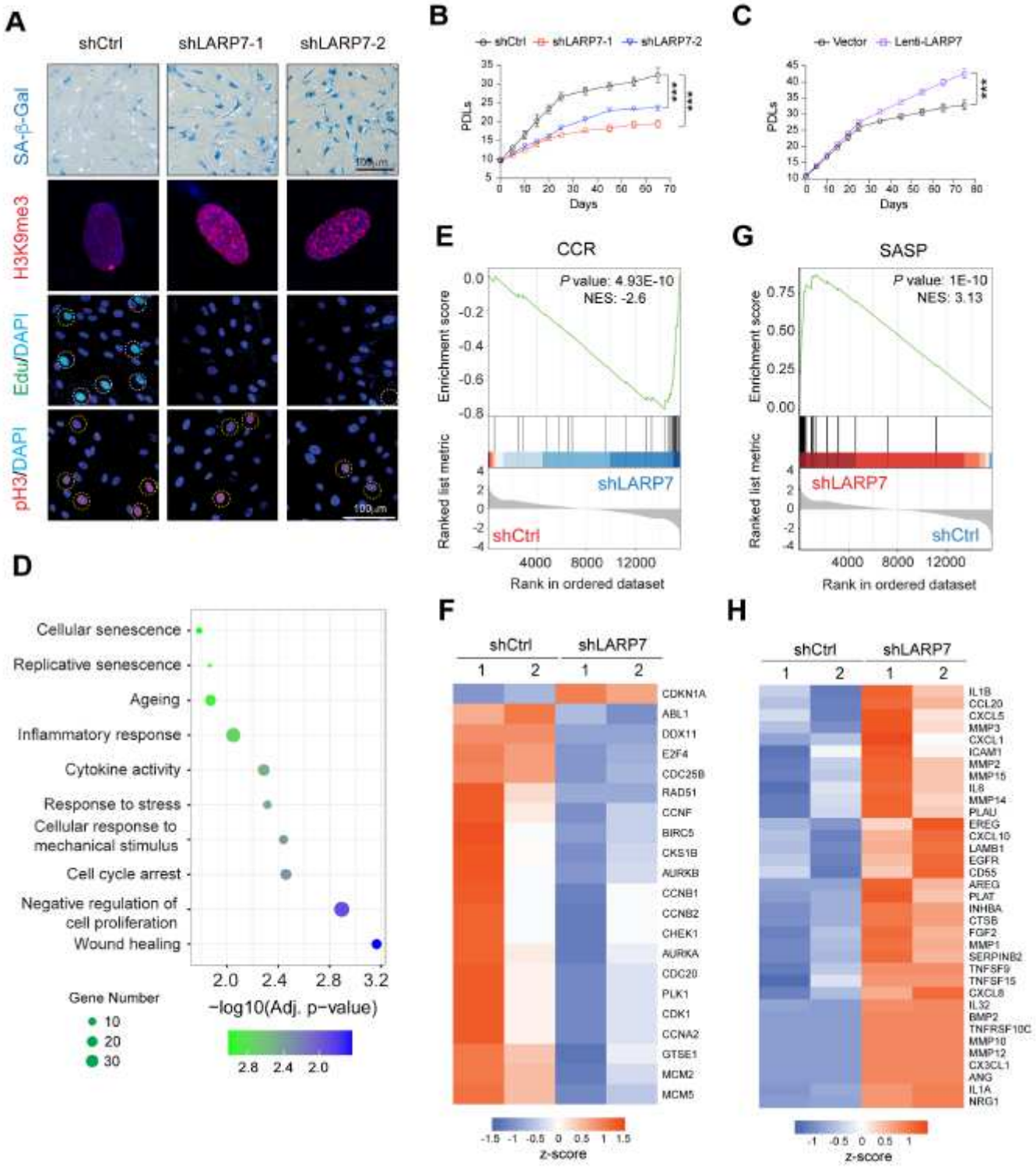

Figure 2

LARP7 depletion accelerated cellular senescence. (A) Histological analysis showing LARP7-depleted IMR90 stable cell lines generated by two independent shRNA exhibited the increased senescence-associated b-Galactosidase activity (SA-b-Gal) and heterochromatin foci (SAHF), and decreased DNA replication (Edu) and cell division activity (pH3). SAHF were revealed by H3K9me3 immunofluorescent staining. Yellow dash circles indicated Edu or pH3 positive nuclei. The statistical quantifications were in Supplemental Figure 2B. (B) Population doubling analysis showing LARP7-depleted IMR90 cells had

declined proliferative potency. PDL denoted population doubling level. (C) Population doubling analysis showing LARP7 overexpression increased the proliferative potency of IMR90 cells. (D) GO analysis of DEG in LARP7-depleted IMR90 cells. (E) Gene Set Enrichment Analysis (GSEA) illustrating the enrichment of cell cycle regulators in LARP7-depleted IMR90 cells. NES: normalized enrichment score. $P<0.05$ indicated significance. (F) Heat map of altered cell cycle regulators in LARP7-depleted IMR90 cells. (G) Gene Set Enrichment Analysis (GSEA) illustrating the enrichment of SASP genes in LARP7-depleted IMR90 cells. NES: normalized enrichment score. $P<0.05$ indicated significance. (H) Heat map of altered cell cycle regulators in LARP7-depleted IMR90 cells. All quantifications in this figure were presented as Mean ± SD. Statistical analysis: the PDL curves were analyzed by linear regression. ***: $P<0.001$.

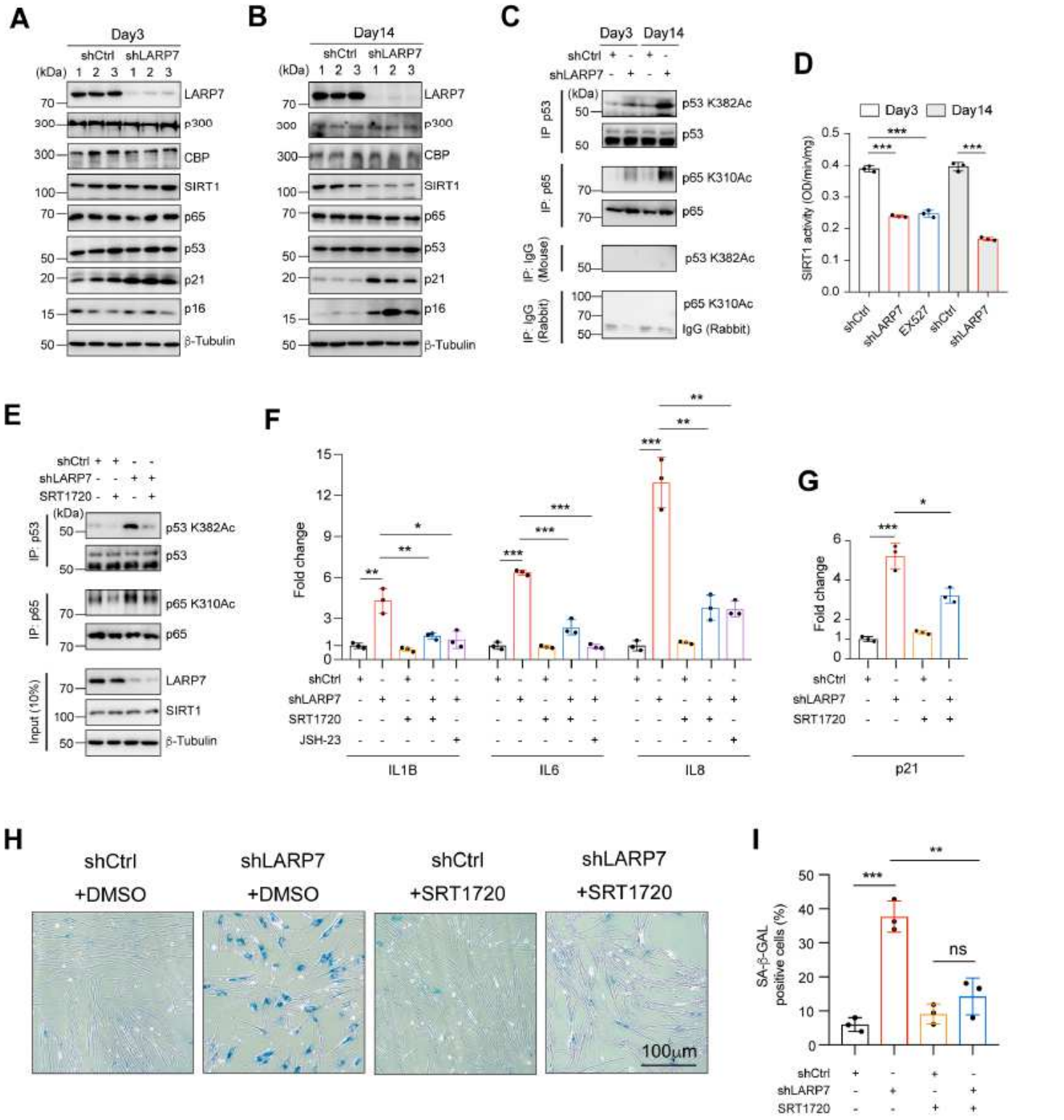

Figure 3

The declined SIRT1 deacetylase activity accounted for LARP7-induced senescence. (A) Western blotting assessing the senescent regulators in IMR90 receiving LARP7 shRNA knockdown for 3 days. (B) Western blotting assessing the senescent regulators in IMR90 receiving LARP7 shRNA knockdown for two weeks. (C) LARP7 knockdown for 3 and 14 days in IMR90 cells increased the acetylation on specific lysine residues of p53 (K382) and p65 (K310). The acetylation of p53 (K382) and p65 (K310) were detected by

acetylation-specific antibody after immunoprecipitated with p53 and p65 antibody. The control IgG (rabbit for p65 and mouse for p53) didn't pull down neither p53 or p65 indicating the specificity of immunoprecipitation. (D) Knocking down LARP7 suppressed the SIRT1 deacetylase activity on both Day3 and 14. 10 μM EX527 inhibitor specific for SIRT1 was used as a positive control. (E) The increased p53 and p65 acetylation upon LARP7 depletion were blocked by SIRT1- specific agonist SRT1720. shCtrl- or shLARP7-transfected IMR90 cells were treated with 1 μM SRT1720 for 12 hours and then subjected to immunoprecipitation. (F) RT-qPCR showing SRT1720 abrogated the SASP gene activation. 2 μM JSH-23, the specific inhibitor for NF-kB, treated IMR90 cells for 48h, and was used as positive control. n=3. (G) RT-qPCR showing SRT1720 abrogated p21 induction in LARP7-depleted IMR90 cells. (H-I) SA-b-Gal staining demonstrated that SRT1720 effectively halted the LARP7 depletion induced senescence. 1 μM SRT1720 were applied to IMR90 cells for 2 days before SA-b-Gal staining (H), and the percentage of SA-b-Gal positive cells were quantified (I). n=3 independent experiments. All quantifications in this figure were presented as Mean ± SD. Statistical analysis: unpaired two-tailed student's t test. *: $P<0.05$, **: $P<0.01$, ***: $P<0.001$. ns: no significance.

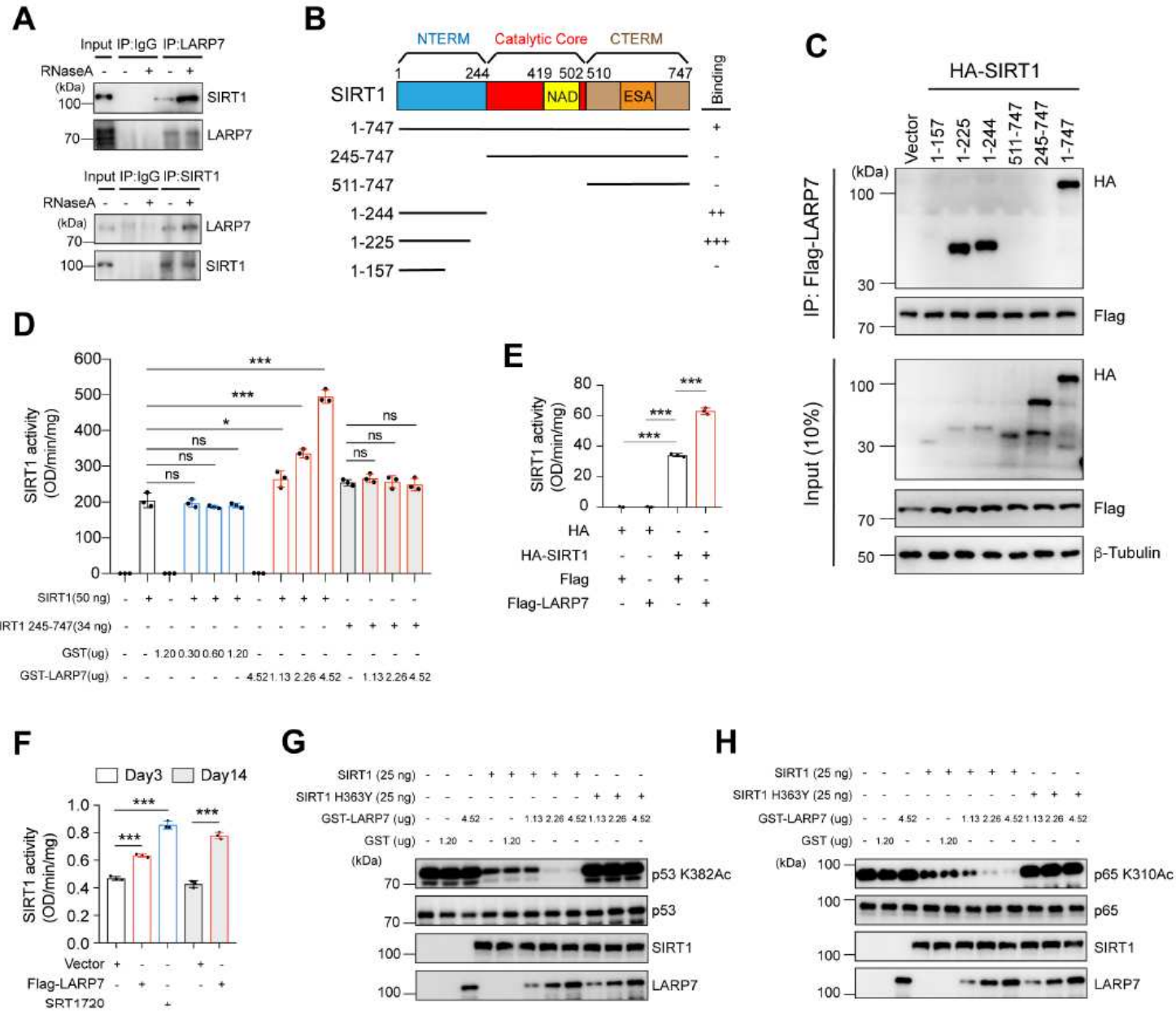

Figure 4

LARP7 enhanced SIRT1 deacetylase activity by directly interacting with its N terminal activation domain. (A) LARP7 interacted with SIRT1 in IMR90 cells as assessed by immunoprecipitation with LARP7 (Top) and reciprocal immunoprecipitation with SIRT1 (Bottom). The 5 μg/ml RNase A was subjected to nuclear protein lysis to remove 7SK RNA, and the results indicted SIRT1- LARP7 interaction is independent of 7SK RNA. (B) Schematic diagram showing functional domains of SIRT1, domain deletions and binding affinity between LARP7 and SIRT1 domain deletions. (C) Domain deletion assay in 293T cells indicated LARP7 interacted with SIRT1 N-Terminal domain (157-244). (D) In vitro SIRT1 deacetylase activity assay showing LARP7 augmented SIRT1 activity in a dose-dependent mean, which required the N-Terminal allosteric activation domain of SIRT1. GST-LARP7, SIRT1 and SIRT1 (245-747) were expressed in E.Coli BL21 (Supplemental Figure 3D), and SIRT1 activity assay kit was used to measure SIRT1 deacetylase

activity. (E) In vitro SIRT1 activity assay demonstrated LARP7 enhanced the intracellular SIRT1 enzymatic activity. Flag-LARP7 and HA-SIRT1 were purified from 293T cells. (F) LARP7 overexpression promoted SIRT1 activity in vivo. IMR90 cells were transfected with indicated constructs or treated with SRT1720 (1μM) for 12 h. (G-H) In vitro deacetylation assay showing LARP7 enhanced SIRT1-mediated deacetylation of p53 and p65. The acetylated p53 (G) and p65 (H) were generated by reacting with histone acetyltransferase p300, and validated by p65 (K310Ac) and p53 (K382Ac) specific antibody (Supplemental Figure 3F, G). All the data in this figure are plotted in Mean ± SD. Two-tailed Student's t test was used for the statistical analysis. Data reflecting three independent experiments. *: $P<0.05$, **: $P<0.01$, ***: $P<0.001$.

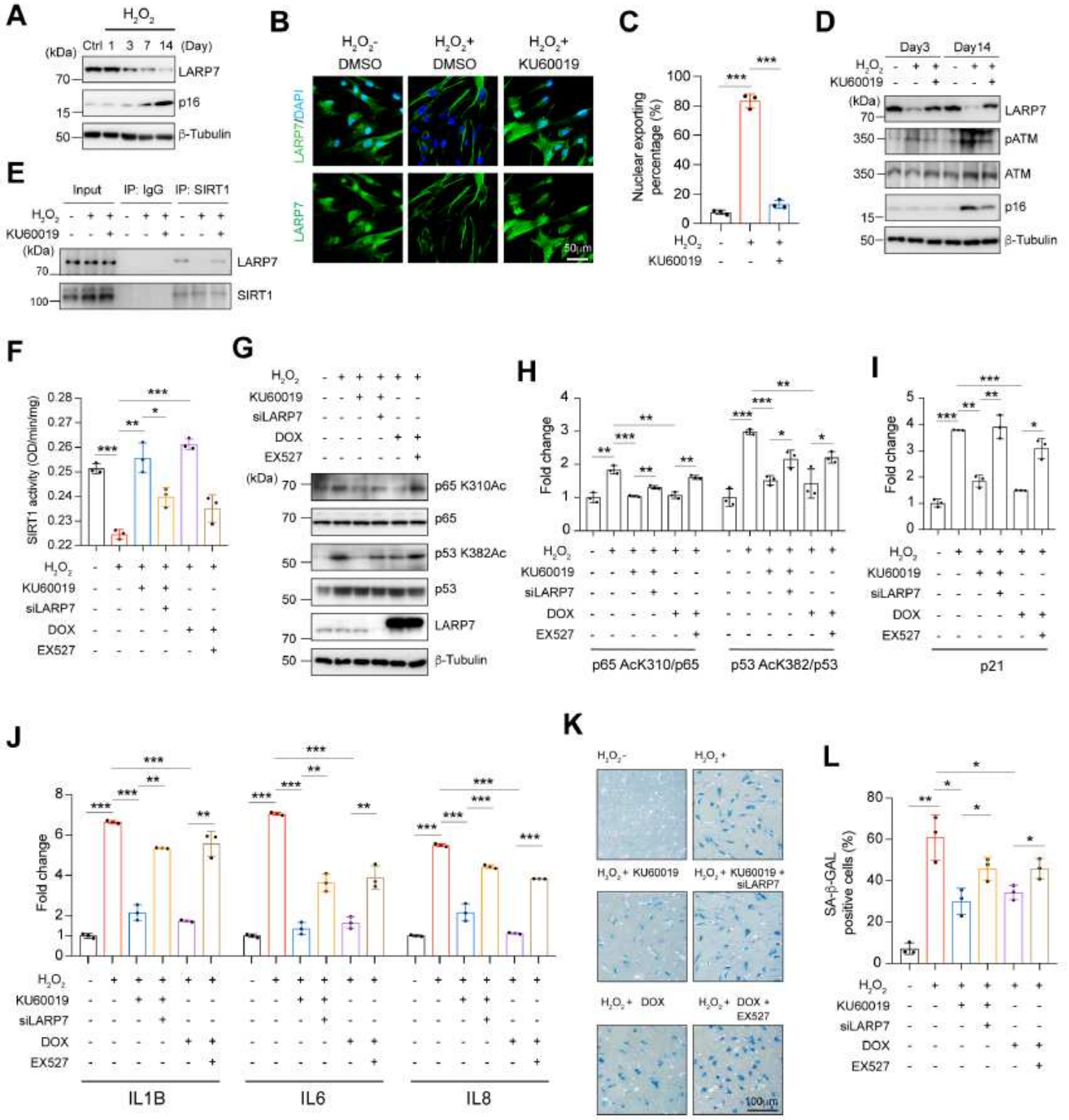

Figure 5

ATM-LARP7-SIRT1 axis mediated DDR-induced cellular senescence. (A) Western blotting showing LARP7 was downregulated after H2O2 treatment. IMR90 cells were exposed to 100 μM H2O2 for 2 hours. (B-C) Immunofluorescence staining showing LARP7 was shuttled out of nuclei upon H2O2 treatment and which was prevented by KU60019. Cells were stained with LARP7 specific antibody 6 h after H2O2 treatment (B), and the percentage of extranuclear exportation was calculated (C). n=3 independent

experiments. (D) ATM mediated LARP7 degradation induced by H2O2. ATM inhibitor KU60019 (10 μM) was pre-incubated with IMR90 cells 2 h before adding 100 μM H2O2. (E) Immunoprecipitation illustrated that H2O2 disrupted LARP7-SIRT1 interaction in IMR90 cells, and which was reversed by ATM inhibition. (F) SIRT1 activity assay in IMR90 cells showing H2O2 repressed SIRT1 activity, which was blocked by ATM inhibition or ectopic expression of LARP7. ATM inhibition reversed SIRT1 activity depending on LARP7 as revealed by siLARP7. IMR90 cells were treated with KU60019 (10 μM) or doxycycline (1 μg/ml, to induce LARP7) or EX527 (10 μM, a SIRT1 inhibitor). (G-H) ATM inhibition or doxycycline-induced LARP7 overexpression abolished H2O2-induced p65 and p53 acetylation. IMR90 cells were pretreated with KU60019 (10μM) or doxycycline (1 μg/ml) or EX527 (10 μM), and then with 100 μM H2O2 for 2 hours. 24 hours after washing out H2O2, the cells were subjected to WB for testing (G) and the blots were quantified with image J (H). n=3 independent experiments. (I-J) ATM inhibition or LARP7 overexpression abolished H2O2-induced p21 and SASP expression. p21 (I) and SASP (J) were measured with RT-qPCR 14 days after H2O2 treatment. n=3 independent experiments. (K-L) SA-b-Gal staining showing KU60019 and LARP7 overexpression reversed the H2O2- induced cellular senescence. IMR90 cells were treated with KU60019 (10 μM) or doxycycline (1 μg/ml, to ectopically express LARP7) or EX527 (a SIRT1 inhibitor, 10 μM) for 14 days before subjected to SA-b-Gal staining and quantified with image J. n=3 assays. All the data in this figure were plotted in Mean ± SD. Two-tailed Student's t test was used for the statistical analysis. *: P<0.05, **: P<0.01, ***: P<0.001.

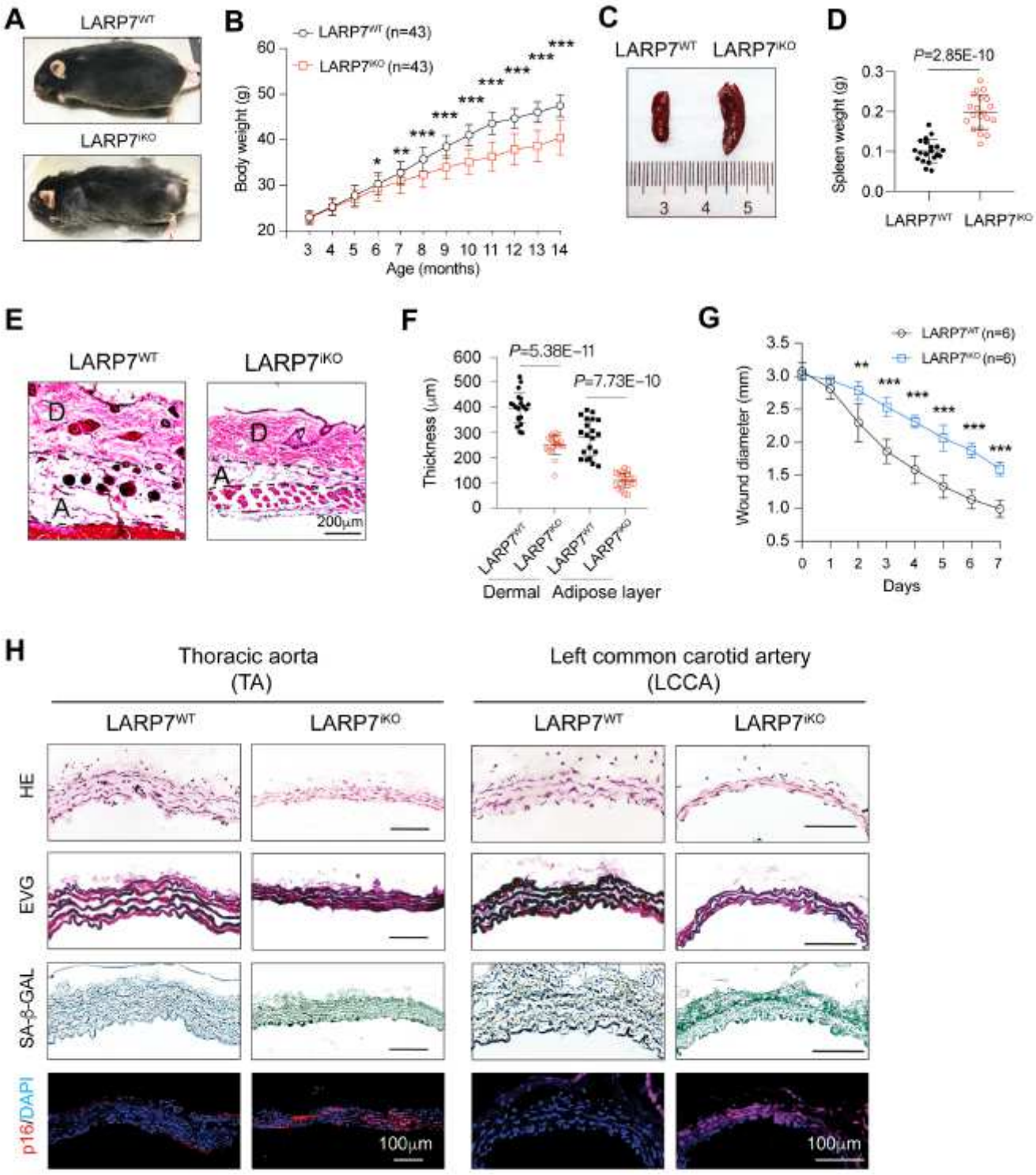

Figure 6

LARP7 deficiency induced the premature aging in vivo. (A) Photographs of 14-month-old LARP7iKO mice illustrating a premature aging phenotype comparing to wildtype littermates. (B) Growth curves of LARP7iKO mice and uninduced control mice. n=43 mice in each group. (C) Representative figure of spleen of 14-month-old LARP7WT and LARP7iKO mice. (D) Statistical analysis of spleen weight of 14-month-old LARP7WT and LARP7iKO mice. (E) HE staining showing the age-related abnormalities in the

skin of LARP7iKO mice. A: subcutaneous adipose layer, D: dermis. (F) Statistical analysis of the thickness of subcutaneous adipose and dermal layer. n=20 mice. (G) Wound healing curves of 3-mm punch biopsy wounds in 14-month-old LARP7iKO and LARP7WT mice. n=6 mice. (H) Vessel images (HE, EVG, SA-b-Gal and p16 staining) showing age-related phenotypes in the thoracic aorta and left common carotid artery of 14-month-old LARP7iKO mice. TA: thoracic aorta, LCCA: left common carotid artery. EVG staining is to reveal the elastic fiber using Elastic stain kit. All plot data were presented as Mean ± SD. The comparison of 6-month-old mice weight in 6B was using Mann-Whitney U test, the others were tested with two-tailed student's t test. *: P<0.05, **: P<0.01, ***: P<0.001.

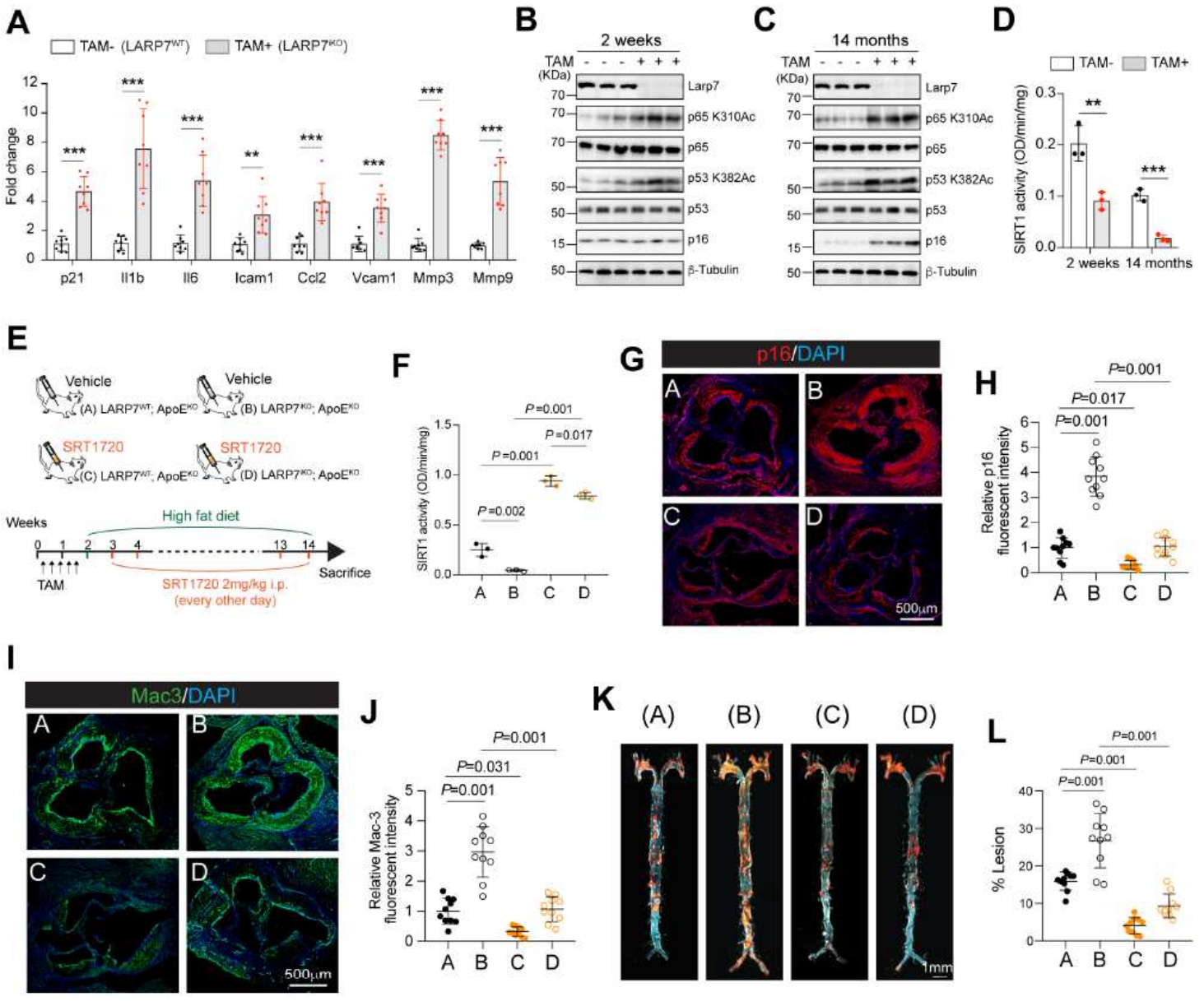

Figure 7

LARP7 deficiency accelerated vascular senescence and atherogenesis in ApoEKO mice by attenuating SIRT1 deacetylase activity. (A) SASP genes and p21 were upregulated in LARP7iKO aortas 14 months after TAM induction. n=8 mice. (B) Aortas of LARP7iKO mice showing elevated acetylation of p65 and

p53 after depletion of LARP7 for 2 weeks. (C) Elevated acetylation of p65 and p53 in aorta after depletion of LARP7 for 14 months. p16 elevated significantly in LARP7-depleted aortas indicated accumulated senescence. (D) LARP7 depletion significantly attenuated the SIRT1 activity in the aortas especially 14 months after induction. n=3 mice. (E) The dose strategy of SRT1720 and HFD for LARP7WT; ApoEKO and LARP7iKO; ApoEKO mice. 50 mg/kg TAM were intraperitoneally injected every other day for 5 times to eliminate LARP7 before treating with SRT1720 and HFD. For SIRT1 activation, 2 mg/kg SRT1720 or vehicle solution (2% DMSO + 30% PEG300 + 1% Tween80) were intraperitoneally injected every other day for 3 months. (F) SIRT1 activity assays illustrating SIRT1 deacetylase activity decreased in aortas of LARP7iKO; ApoEKO mice, and SRT1720 significantly elevated the SIRT1 activity in both LARP7WT; ApoEKO and LARP7iKO; ApoEKO mice aortas. n=3 aortas. (G-H) p16 staining showing LARP7 depletion increased the senescent cells accumulation in the atherosclerotic lesion of ApoEKO mice, but which was mitigated by SRT1720. n=10 aortas. (I-J) Mac3 staining to unveil the infiltrated macrophages and inflammatory status in aortic roots. Representative staining images (I) and relative Mac3 fluorescent intensity (all versus ApoEKO group A, J) were presented. n=10 aortas. (K-L) LARP7 depletion increased the atherogenesis which was reversed by the treatment with SRT1720. The representative images of atherosclerosis lesions of aorta en face stained by oil red (K). The calculation of percentage of lesion area relative to total region (L). n=10 mice for each group. All plots were presented as Mean ± SD, Figure 7D was tested with two-tailed student's t test, the rest plots were tested with one-way ANOVA followed by Tukey post-hoc test. $P<0.05$ indicated significance.

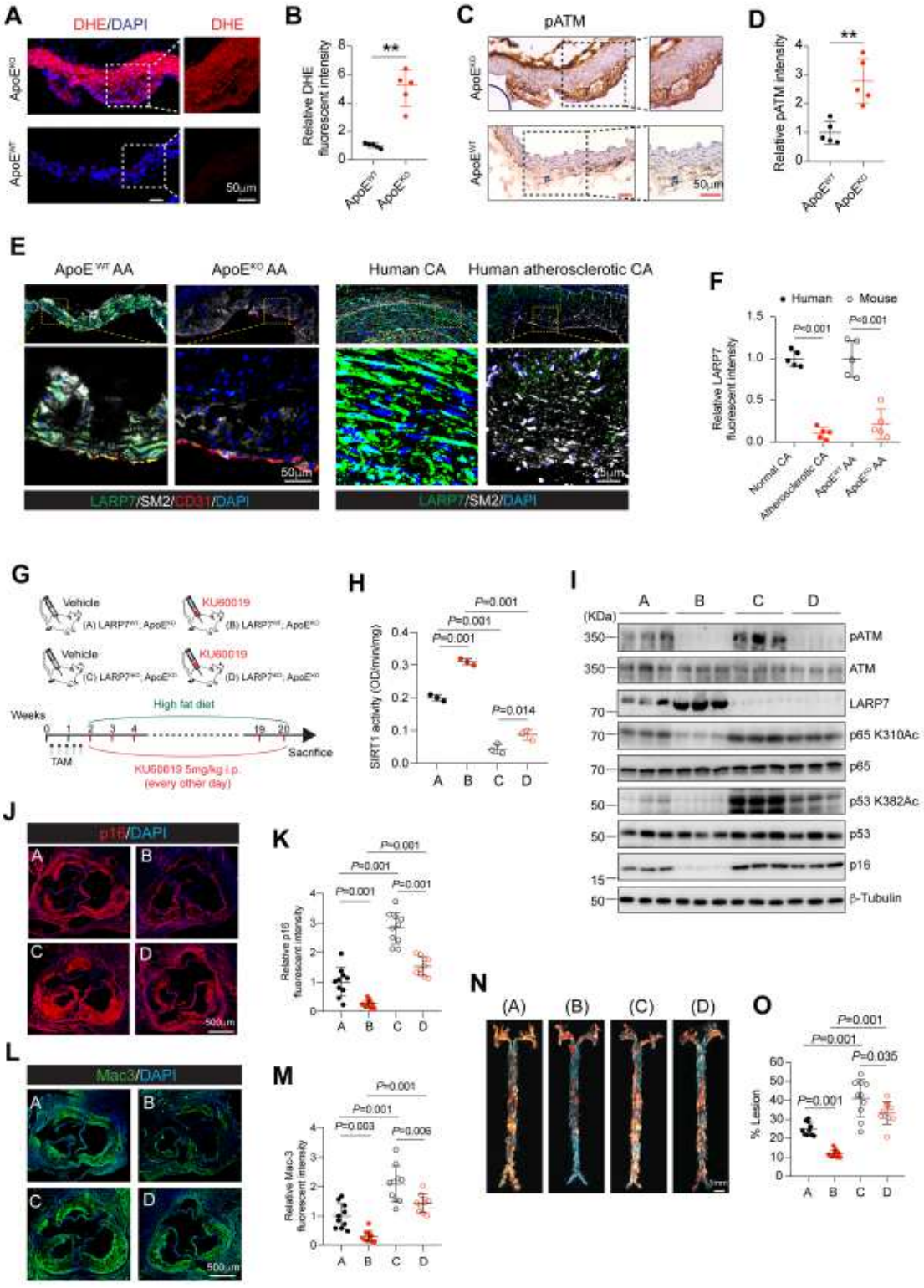

Figure 8

ATM inhibition alleviated vascular senescence and atherogenesis. (A-B) Dihydroethidium (DHE) staining illustrating elevated ROS in the atherogenic aorta. Freshly isolated aorta from ApoEWT and ApoEKO mice receiving HFD for 8 weeks were stained with DHE (A), and the staining density was quantified with ImageJ (B). n=5 aortas. (C-D) Immunohistochemistry of phosphorylated ATM illustrated the hyperactivation of ATM pathway in atherogenic aorta. The aorta from ApoEKO mice receiving HFD for 2

months were applied for the pATM staining (C), and pATM intensity was quantified with ImageJ (D). (E-F) Immunofluorescence staining showing LARP7 markedly declined in atherosclerotic lesions of arch aorta of ApoEKO mice and human coronary artery. The atherogenic arch aorta was isolated from ApoEKO mouse receiving HFD for 2 months. Human normal and atherogenic coronary arteries were obtained from the patients receiving heart transplantation. The LARP7 fluorescent intensity was calculated with ImageJ (F). CA: coronary artery; AA: arch aorta. n=5. (G) The strategy for KU60019 administration. 5 mg/kg KU60019 were intraperitoneally injected to LARP7WT; ApoEKO and LARP7iKO; ApoEKO mice for 18 weeks. (H) The SIRT1 activity in the aortas of LARP7WT; ApoEKO and LARP7iKO; ApoEKO mice treated with or without KU60019. n=3 aortas. (I) Western blotting showing ATM inhibition decreased p16 expression and the acetylation of p53 and p65 in LARP7WT; ApoEKO mice aorta, but which were comprised by the further knocking out LARP7. LARP7WT; ApoEKO and LARP7iKO; ApoEKO mice were fed with HFD for 18 weeks. (J-K) p16 immunofluorescent staining showing KU60019 prevented the senescent cells accumulation in the aortic root, but which was compromised by knocking out LARP7. p16 fluorescent intensity from 10 aortic roots were calculated (K). (L-M) Mac3 immunofluorescent staining of aortic root. The cryosection of aortic root was stained with Mac3 antibody (L), and the fluorescent intensity was calculated with ImageJ (M). n=10 mice. (N-O) KU60019 markedly alleviated the atherogenesis of LARP7WT; ApoEKO mice, but which was compromised by knockout of LARP7. The oil red staining of the aorta en face (N) was quantified as the percentage of lesion in total aortic area (O). n=10 aortas. All plots were presented as Mean ± SD, Figure 8B, D and F was tested with two-tailed student's t test, the rest plots were tested with one-way ANOVA followed by Tukey post-hoc test. $P<0.05$ indicated significance.

Supplementary Files

This is a list of supplementary files associated with this preprint. Click to download.

- SupplementaryTable1RNASeq.xlsx
- SupplementaryTable2Oligo.xlsx
- SupplementaryTable3Atheosclerosisstudy.xlsx
- SupplementaryTable4Antibody.xlsx